Bulk and surface laser damage of silica by picosecond and nanosecond pulses at 1064 nm

Arlee V. Smith[1,*] and Binh T. Do[2]

[1]Department 1128, Sandia National Laboratories, Albuquerque, New Mexico 87185-1423, USA

[2]Ball Aerospace and Technologies Corporation, Albuquerque, New Mexico 87106, USA

*Corresponding author: arlee.smith@as-photonics.com

Received 2 May 2008; accepted 21 July 2008;
posted 4 August 2008 (Doc. ID 95705); published 9 September 2008

We measured bulk and surface dielectric breakdown thresholds of pure silica for 14 ps and 8 ns pulses of 1064 nm light. The thresholds are sharp and reproducible. For the 8 ns pulses the bulk threshold irradiance is $4.75 \pm 0.25\,\mathrm{kW}/\mu\mathrm{m}^2$. The threshold is approximately three times higher for 14 ps pulses. For 8 ns pulses the input surface damage threshold can be made equal to the bulk threshold by applying an alumina or silica surface polish.

OCIS codes: 140.3330, 060.2290, 190.5940, 190.5890.

1. Introduction

The customary description of the bulk damage mechanism for picosecond and nanosecond light pulses is an electron avalanche driven by the electric field of the laser light, followed by an energy transfer from hot electrons to the glass or crystal matrix, which causes melting or fracturing. The electron avalanche starts with one or more conduction band electrons. If the optical field oscillates with a period much shorter than the time between momentum changing collisions for the electrons, an electron merely oscillates in place with few collisions with the matrix and without extracting much energy from the field. However, if the electron collides with the matrix many times during each optical cycle, it will gain energy (inverse bremsstrahlung), eventually acquiring sufficient kinetic energy to free a second electron. Both of these electrons are then heated until they liberate two more electrons and so on. As the electron density approaches the critical plasma density n_e,

$$n_e = \omega^2 m_e^* \epsilon_\circ / e^2 \approx 10^9\ \mathrm{electrons}/\mu\mathrm{m}^3, \qquad (1)$$

the laser light is strongly absorbed, leading to rapid heating of the electron-hole plasma. In Eq. (1) ω is the frequency of the laser light, and m_e^* is the effective mass of an electron. Most of the plasma energy is transferred to the matrix on a nanosecond time scale, and it is sufficient to fracture or melt the matrix.

Estimates of silica's properties support this avalanche model. Silica matrix atoms are approximately 0.25 nm apart, and the velocity of a 5 eV electron is roughly 10^{15} nm/s, making the collision time approximately 0.25 fs. The resulting diffusion distance for 5 eV electrons is roughly $0.5\sqrt{\tau}\ \mu$m, where τ is time in nanoseconds. This simple estimate agrees well with more sophisticated band structure calculations [1]. For an 8 ns light pulse focused to an 8 μm waist, electron diffusion can probably be neglected, because the diffusion length of 1.4 μm is considerably less than the 8 μm beam size. This corresponds to the longest pulses and smallest beam sizes used in this study, and, of course, electron diffusion is even less important for shorter pulses and larger beams. However, if a standing wave is formed by retroreflecting the light beam, the distance between peak and valley of the standing wave is less than 200 nm, so electron diffusion might then be important. Diffusion of heat by phonons is even less important than electron diffusion in our experiments. The thermal diffusion

0003-6935/08/264812-21$15.00/0

distance is only $0.03\sqrt{\tau}$ μm, where τ is in nanoseconds.

Optical breakdown thresholds for surfaces are nearly always reported to be two to five times lower than for the bulk. This reduction might be due to micro fractures near the surface or to scratches on the surface caused by the polishing process. Such microscopic defects can locally enhance the optical field [2] and might initiate a plasma near the defect at lower power than is required in the bulk. Alternatively the lower surface threshold might be due to residual polishing compounds chemically bound to the surface or embedded in the surface.

This general understanding of optical breakdown emerged long ago [2], but in the intervening years many contradictory and confusing observations of the breakdown behavior of silica have been reported. Measured breakdown thresholds vary by a factor of more than 100 for 10 ns pulses. Other important unresolved or confusing issues include scaling of the damage threshold with pulse duration and focal spot size, the roles of stimulated Brillouin scattering (SBS), self-focusing, color center formation, material densification, impurity inclusions, as well as the differences between surface and bulk damage, plus the possibility of annealing or cumulative damage when multiple pulses are used. We thought it worthwhile to take a fresh look at the surface and bulk breakdown of silica to sort myth from reality and to try to reconcile the many apparent contradictions. For example, the importance of self-focusing in breakdown has long been recognized, but some information in the literature is misleading, so we reexamine its influence on damage measurements. On the other hand, the importance of SBS has been less well recognized. We show that it is likely to interfere with damage measurements unless the beam is tightly focused. In Section 2 we discuss in more detail some of the conflicting or confusing observations regarding optical damage of silica.

2. Some Unresolved Questions about the Optical Breakdown of Silica

A. Statistical Versus Deterministic Thresholds

One question with conflicting answers is whether the breakdown threshold of silica is statistical or deterministic. A statistical threshold might reflect variations in the number of free electrons [3] available to initiate an electron avalanche, or it might reflect a statistical distribution of inclusions in silica that might initiate damage [4]. However, Glebov *et al.* [5,6] stated that the bulk damage threshold is deterministic in silicate glasses if the laser pulse is single longitudinal mode and the focal spot is small. They attribute the nearly universally reported statistical nature of the threshold solely to the statistics of the maximum irradiance associated with the multiple short power spikes characteristic of multimode pulses. This is disputed by others [7,8] who claim the bulk damage threshold is statistical, even with single-mode pulses. All surface damage threshold reports we are aware of state that the surface threshold is statistical, perhaps reflecting random distributions of polish-related surface defects.

B. Surface Versus Bulk Damage

In most reports the surface damage threshold is a factor of 2–5 lower than the bulk damage. One contrary observation [9] claims that the surface and bulk damage thresholds are equal in silica when the surface is finely polished. Unfortunately this report did not specify in detail how their surfaces were polished, and furthermore their reported damage thresholds are a factor of 5 lower than we report here.

There is clear evidence that polishing methods affect the surface damage threshold. Silica optics are often polished using a CeO_2–water slurry. It is well established that this leaves a thin surface layer composed of a mixture of silica and ceria. There is also convincing evidence that the likelihood of damage at a fixed fluence level increases with ceria concentration [10]. Other polishes, such as Al_2O_3, leave no such layer, and the damage threshold is usually higher than with ceria, but the surface damage threshold is still generally reported to be substantially lower than the bulk. This is usually explained in terms of microscopic subsurface damage left by the polishing process or in terms of absorptive inclusions on or near the surface. The subsurface damage might be gouges or cracks, and these tend to magnify the local irradiance by a factor up to n^4, where n is the refractive index ($n = 1.45$). Damage would start at such spots and spread, so the silica surface threshold irradiance or power could be reduced by a factor of 4–5 compared with the bulk threshold [2,11]. A random distribution of microscopic damage would also explain a statistical surface damage threshold. Presumably the density of surface defects could be reduced by a finer final polish, and this appears to be the case for fine alumina polishes. A meaningful evaluation of the literature is difficult, because the polishing methods are rarely described in sufficient detail.

We conclude that it is well established that the surface damage threshold depends on the surface polish, but it is less clear whether the surface damage threshold ever equals the bulk threshold. It is also unclear whether it is possible to observe an intrinsic surface damage threshold and, if so, whether it is statistical or deterministic.

C. Conditioning Versus Cumulative Damage

In some materials the damage threshold decreases after exposure to multiple subthreshold pulses. This could reflect an accumulation of material damage such as color center formation. In other materials the threshold appears to rise with exposure to subthreshold pulses. This could be due to annealing of defects by intense light. Most reports [6,12,13] find no evidence of either effect in bulk silica. However, some [14,15] report evidence of cumulative damage. They find that accumulation of damage is less significant at one pulse per second than at ten pulses per second, indicating a transient fatigue. They also find multiple pulse damage accumulation is more significant for bluer light than for redder light, and they suggest that electrons excited to the conduction band might be trapped in high lying levels that are easily ionized on successive pulses, and that this trapped population could build over many pulses. They conclude that different mechanisms must govern single and multiple pulse damage. Chmel [16] reviewed this issue and observed that cumulative damage seems to be associated exclusively with multilongitudinal-mode pulses, hinting that it may be a phantom related to the statistical variations inherent to multimode pulses.

D. Beam Size Effect

Some papers [6,12,14,15] report a strong decrease in the bulk damage threshold fluence with increasing beam size. This might be attributed [12] to the larger number of free electrons available to initiate an avalanche in a larger focal volume. The question of a size effect was also reviewed by Chmel [16], who noted that cumulative damage effects appear to be smaller for a smaller focal volume. We point out that larger focal spots imply that higher powers are required to cause damage, and this means self-focusing and SBS are more likely to complicate threshold measurements.

E. Electron Avalanche Versus Alternative Damage Mechanisms

The usual model of optical damage of silica by picosecond and nanosecond pulses involves an electron avalanche as described in our introduction. This process is similar to dielectric breakdown by a DC electric field, so we would expect the breakdown optical field to be roughly equal to the DC breakdown field. Based on what we judge a reliable DC threshold [17], this implies a threshold irradiance of approximately $5\,\mathrm{kW}/\mu\mathrm{m}^2$ ($500\,\mathrm{GW/cm}^2$), but most reported damage thresholds for 10 ns pulses are a factor of 100 lower than this, casting doubt on the electron avalanche explanation. However, there are several reports of measured damage irradiances that fall in the intervening range from 1 to 100 times below $5\,\mathrm{kW}/\mu\mathrm{m}^2$, and most reported thresholds for picosecond pulses lie close to the expected irradiance. For femtosecond pulses, in contrast, the time is too short for an avalanche to fully develop, and multiphoton ionization assumes nearly equal importance to the avalanche. A review of damage by femtosecond pulses is outside the scope of this paper, except to note that models that combine avalanche and photoionization agree reasonably with femtosecond measurements, and that femtosecond damage typically occurs at the input surface and is deterministic.

The avalanche model is not without doubters. Some claim that picosecond–nanosecond damage is due not to electron avalanche but rather to a thermal runaway [18,19], and the Shen *et al.* [20] observation that there is no observable electron avalanche below the threshold damage irradiance is cited in support of this. The thermal explanation assumes that a silica surface defect or an absorbing bulk inclusion is heated by the laser light, and in turn it heats the surrounding silica. If the optical absorption coefficient of the surrounding silica increases with temperature, this could lead to a rapid thermal runaway that causes melting and fracture. A statistical distribution of surface defects and bulk inclusions would explain the reported statistical variations in the damage threshold fluence.

F. Wavelength Effect

The simple picture of an electron avalanche due to heating of free electrons by the optical field implies the damage threshold fluence should increase slightly as the wavelength decreases, because bluer light is less effective in heating electrons since there are fewer velocity changing collisions during each optical cycle. However, some researchers [4,15,21–23] report that the damage threshold fluence falls with decreasing wavelength over the range of 1064–266 nm. These observations seem to indicate that effects other than avalanche ionization are important. Multiphoton ionization presumably would scale in the observed direction, so perhaps it is more important than anticipated. Lattice defects also produce much stronger absorption in the blue than at 1064 nm, so they might be responsible for this trend.

G. Strain Effect

Mechanical strain is important in optical fibers where it is used to induce birefringence in polarization-maintaining fiber. There is some evidence that damage thresholds change with strain [24]. It is important to know whether strain affects the damage threshold at the relatively low strain levels encountered in fiber.

H. Stimulated Brillouin Scattering Effect

The SBS threshold power for a tightly focused beam is nearly independent of the size of the focal waist, provided the focus lies deep inside the sample. However, reaching the damage threshold demands higher power with increasing focal size. These two facts imply that for focal waists larger than a certain size, the SBS threshold power is always exceeded before damage occurs.

SBS could affect a damage measurement in contrasting ways, depending on the circumstances. In some cases SBS protects the focus by reflecting the incoming energy in the form of the Stokes wave, thus keeping the full irradiance from reaching the focus [25,26], and this raises the apparent damage threshold. However, for a focus near the input face, this protection does not apply. Instead the Stokes wave interferes with the incoming pump wave to form a moving interference pattern. At a fixed location this field oscillates at the acoustic frequency of approximately 15 GHz for 1064 nm light, with antinodes substantially stronger than the incoming wave.

Assuming damage occurs on a time scale shorter than the acoustic oscillation period of 60 ps, this reduces the apparent damage threshold by a factor of 4 or possibly even more if the Stokes wave can focus as it approaches the input face.

The role of SBS in damage by nanosecond pulses has been suspected [27] but not definitively demonstrated. For weakly focused beams with a diameter less than 1 cm, this would tend to produce front surface damage as is commonly observed. For multicentimeter diameter beams, it has been demonstrated that the SBS gain of a transverse Stokes wave can be large enough to cause damage [28].

I. Self-Focusing Effect

Self-focusing in bulk dielectrics has been well understood for many years [29,30]. Briefly, there is a critical self-focusing power, P_{SF}, that is approximately 4.3 MW for linearly polarized 1064 nm light in silica. For powers greater than P_{SF}, a beam with a perfect Gaussian profile will self-focus to a tiny diameter, making optical damage inevitable. This constriction develops over a distance on the order of a Rayleigh range, however, so self-focusing does not always occur within the sample simply because P_{SF} is exceeded. Even for powers below P_{SF}, incipient self-focusing causes the focal waist to shift and constrict, enhancing the irradiance at the waist. Self-focusing is complicated somewhat by the presence of fast (Kerr) and slow (electrostrictive) contributions. For beam profiles other than a lowest order Gaussian, the influence of self-focusing beams must be analyzed using numerical beam propagation methods. Unfortunately, in many reports on damage, self-focusing is ignored or misinterpreted. It may play a role in the size effect mentioned above.

J. Pulse Duration Effect

The most perplexing claims in the damage literature concern scaling of the damage threshold fluence with pulse duration. Tien *et al.* [31] measured the breakdown fluence for 800 nm light with pulse durations ranging from 20 fs to 7 ns and found that over the range of 20 ps to 7 ns, the threshold fluence varies as $\tau^{0.5}$. Their value for the threshold fluence at 7 ns is 200 J/cm^2. Similarly Du *et al.* [32] found the damage fluence for 780 nm light is proportional to $\tau^{0.5}$ over the range of 10 ps to 7 ns, with a comparable 7 ns value of 200–500 J/cm^2. Stuart *et al.* [33] also report a $\tau^{0.5}$ dependence for 1013 nm light over the 10 ps to 1 ns range, with a projected threshold fluence of 100 J/cm^2 at 7 ns. All three of these measurements were for surface damage, so they do not necessarily apply to bulk damage. They were each made using femtosecond pulses stretched to variable durations and amplified. Whether this produced temporally smooth stretched pulses is not entirely clear from the reports. However, the phase modulated pulses should strongly suppress SBS.

Campbell *et al.* [34] summarize a large number of measurements of silica damaged by 1 to 100 ns pulses of 1060 nm light with a $\tau^{0.4}$ scaling of the damage threshold. Their damage fluence for 7 ns pulses is 50 J/cm^2. The pulses in this study are sometimes spectrally narrow, so SBS could be a factor. Van Stryland *et al.* [12] also claim a $\tau^{0.5}$ dependence for bulk damage produced by tightly focused beams with durations from 40 ps to 30 ns. Taken together these reports of duration scaling form an impressive array of measurements, most of them referring to surface damage, and all claiming a similar scaling law. However, no compelling explanation of this law is offered.

Figure 1 shows these duration scaling results along with several other 1064 nm thresholds measured for fixed pulse durations. For durations near 10 ns the measured thresholds vary by a factor of 100 from the variable duration studies up to the avalanche threshold deduced from the DC breakdown field. Clearly most of the thresholds fall far below the value extrapolated from the DC breakdown value. In some cases the low values could be due to the lack of self-focusing corrections. Alternatively, the generally low values might indicate that the damage process is something other than electron avalanche. Rubenchik and Feit [19] and also Stuart *et al.* [23] attribute surface damage induced by ultraviolet light to the presence of nanoscale absorbing defects near the surface that are associated with polishing, and damage is presumed to be due to a thermal runaway combined with avalanche ionization. The $\sqrt{\tau}$

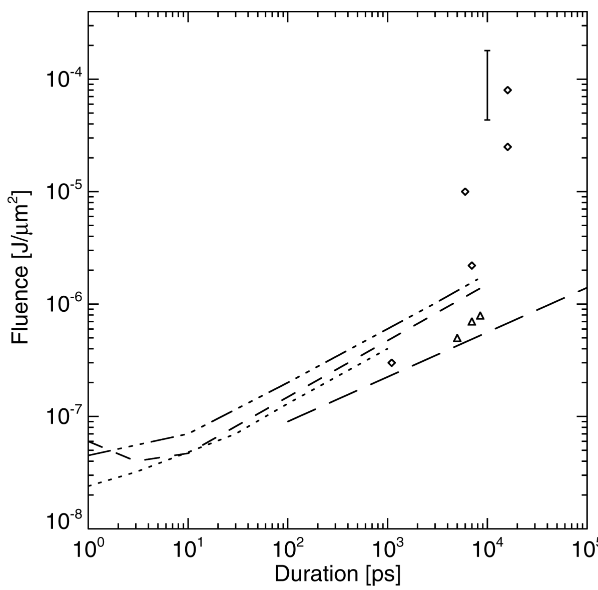

Fig. 1. Summary of reported damage threshold fluences for silica with picosecond and nanosecond pulses. The vertical bar indicates a threshold range for an electron avalanche, deduced from the DC electric field breakdown threshold reported by Yasue *et al.* [17]. The lines, bottom to top at 1 ns, are reported thresholds from studies of pulse duration scaling by Campbell *et al.* [34], Stuart *et al.* [33], Du *et al.* [32], and Tien *et al.* [31]. The triangles (surface damage) and diamonds (bulk damage), lowest to highest fluence, are from Kuzuu *et al.* [22], Krol *et al.* [61], Natoli *et al.* [62], Kamimura *et al.* [63], Natoli *et al.* [64], Webster *et al.* [8], and Kitriotis and Merkel [14,65].

scaling is associated with the diffusion of heat away from the nanoscale absorbers into the lattice, but it is necessary to assume a particular distribution of particle sizes to obtain the observed scaling. This explanation is not entirely convincing. Several questions need answers. Why are the back surfaces not damaged first in most studies? Different polishing methods should be studied systematically to test this idea. Has this been done? Does the absorption and heating model apply to 1064 nm as well as ultraviolet light? What is the identity of the absorbers, and is the required size distribution likely? None of the avalanche models reproduce a $\tau^{0.5}$ scaling, and avalanche cannot be assumed at the low damage thresholds usually reported. Nevertheless, the $\sqrt{\tau}$ dependence of damage threshold fluence seems entrenched [35], even for bulk damage. However, the wide range of reported thresholds calls for more measurements using better characterized samples and better characterized laser pulses.

3. Experiment

In our effort to clarify these issues, we use the laboratory setup shown in Fig. 2 to measure bulk and surface damage thresholds for 8 ns and 14 ps pulses in different grades of Corning 7940 fused silica. Our 8 ns laser is an injection seeded, Q-switched Nd:YAG laser that reliably operates on a single longitudinal mode, producing temporally smooth 1064 nm pulses. To make the beam's spatial profile closely approximate a Gaussian, we operate the oscillator with a 1 mm diameter iris inside the laser cavity. This produces a symmetric output beam that we tightly filter using a wire die to produce a nearly perfect Gaussian beam that is then amplified in a single-pass amplifier. The beam is kept small enough to avoid clipping at the edges of the amplifier rod. After amplification the beam is again tightly filtered using a wire die followed by an iris that clips the Airy pattern at its first null. At the sample the beam is spatially smooth and nearly Gaussian in transverse profile. Figure 3 shows typical temporal and spatial profiles. The 14 ps laser is a mode-locked, Q-switched Nd:YAG laser that is likewise spatially filtered to produce a high-quality Gaussian beam.

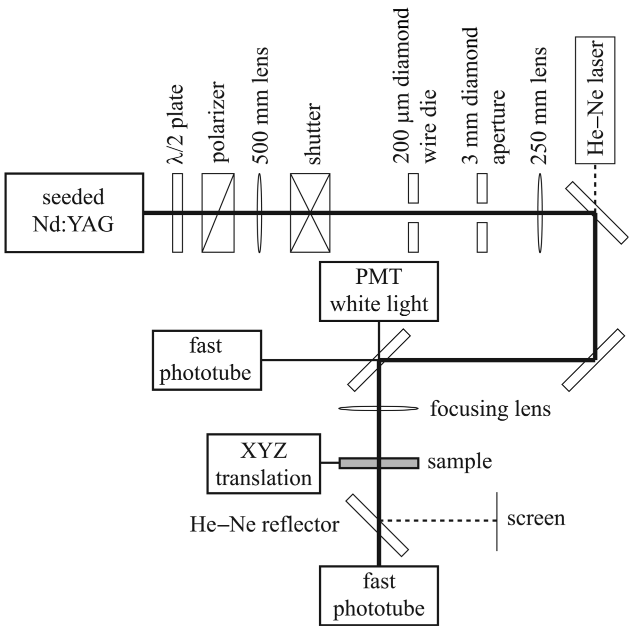

Fig. 2. Diagram of the apparatus used to measure the damage threshold fluence of dielectric samples. The 1064 nm Nd:YAG laser operates on a single longitudinal mode to generate 8–12 ns long pulses with smooth temporal profiles. The beam is attenuated to a few millijoules in the variable attenuator and then spatially filtered by focusing through a diamond wire die followed by a circular aperture to clip all except the lowest-order Airy lobe. The filtered beam's temporal profile is monitored using a fast photo tube. Singlet lenses focus the light to 8–16 μm spots inside the sample, and a photo multiplier detects white light emitted by the sample at fluences above the damage limit. A fast photo tube records the transmitted pulse, and a pilot He–Ne beam probes the focus for damage.

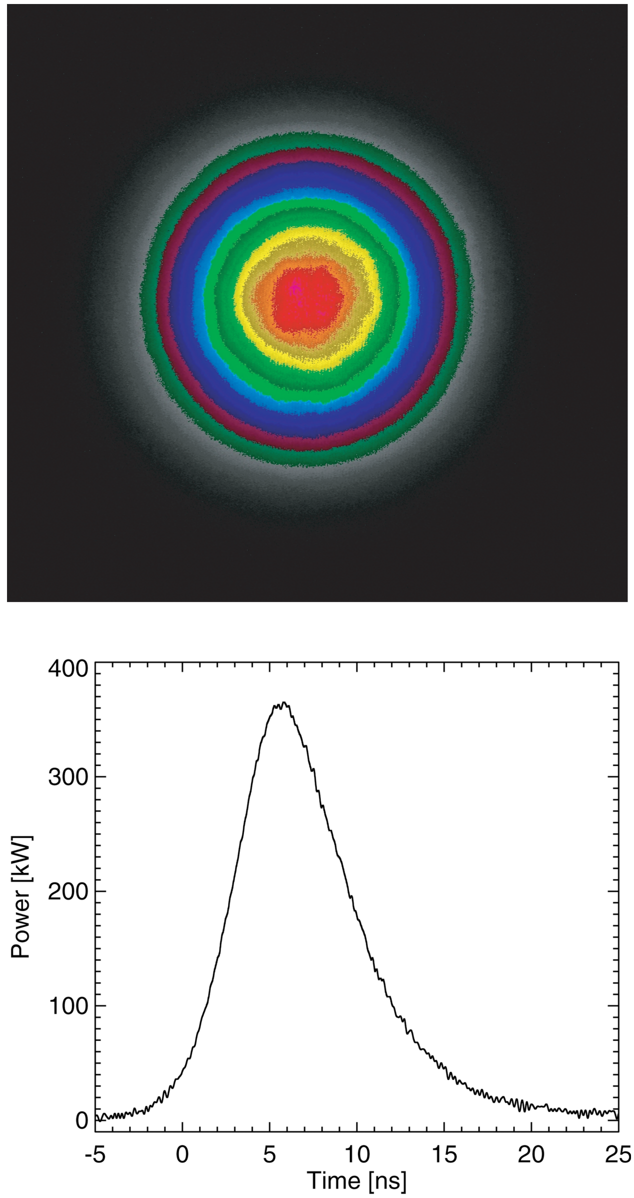

Fig. 3. (Color online) Typical temporal and spatial profiles for the Q-switched laser before focusing into the samples.

The beam is focused into the silica sample by either a 1 or 2 in focal length lens, both of which are double antireflection coated, best-form singlet lenses, giving focal spots of $w_\circ = 8 - 16\,\mu\text{m}$ ($w_\circ$ is the waist radius at e^{-2} irradiance). The sample is held by an xyz positioning stage with submicron resolution in the transverse directions and $5\,\mu\text{m}$ resolution in the longitudinal direction. The entire beam propagation zone, including the sample, is surrounded by an enclosure to avoid beam deflections by air currents. At the sample the beam moves less than $1\,\mu\text{m}$ so reliable multiple pulse measurements are possible.

We verified that the intensity profile is nearly Gaussian in space and time. We measured the spatial profile directly by scanning a knife edge through the beam. The knife edge was attached to the back side of a 1.6 mm thick fused silica sample. Many of our damage measurements used a focal depth of 1.6 mm, so this gives a direct measure of the focal spot in the samples at the actual focal depth. Figure 4 shows knife edge scans in two orthogonal directions. The knife edge measurements require low pulse energy to avoid damage to the knife blade. They are tedious because the waist must be located by making numerous knife edge scans at different z locations. In the example shown in Fig. 4, the waist size is $7.9 \pm 0.1\,\mu\text{m}$ in one plane and $8.0 \pm 0.1\,\mu\text{m}$ in the orthogonal plane.

As an alternative, much faster, and more convenient method of measuring the focal size and positioning the sample relative to the focal waist, we use the method of surface third harmonic generation [36]. The front or rear surface of the sample is scanned through the focus while the forward third harmonic signal is gathered by a photo multiplier. The fundamental power is kept low enough that self-focusing corrections are negligible. Figure 5 shows an example third harmonic trace as the entrance surface is moved through the focus. The third harmonic signal is proportional to w^{-4}, where w is the beam size at the window face, so we fit it to the function

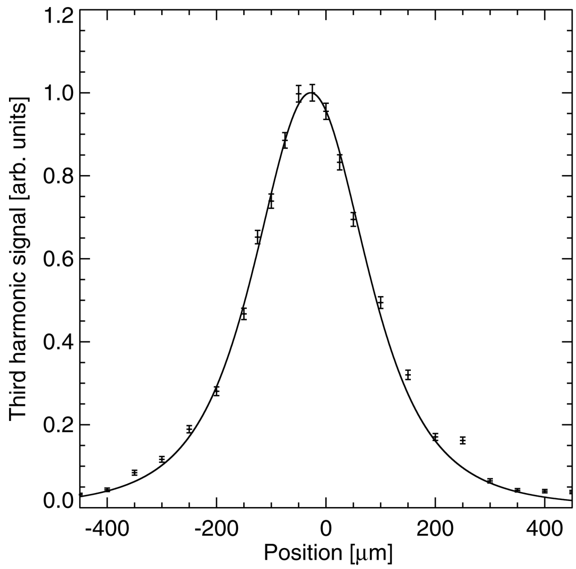

Fig. 5. Third harmonic signal versus position of the entrance face of a fused silica window as it is scanned through the focus. The solid curve is a best fit to the measured values and corresponds to a Rayleigh range of $z_R = 198 \pm 4\,\mu\text{m}$, which implies $w_\circ = 8.2 \pm 0.1\,\mu\text{m}$.

$$S = \frac{S_\circ}{[z_R^2 + (z - z_\circ)^2]^2} \tag{2}$$

to derive the fitting parameters z_R (the Rayleigh range in air), $z_\circ$ (the location of the surface), and $S_\circ$ (an amplitude scaling factor of no interest). The Rayleigh range is related to the beam waist by

$$z_R = \frac{w_\circ^2 k}{2}. \tag{3}$$

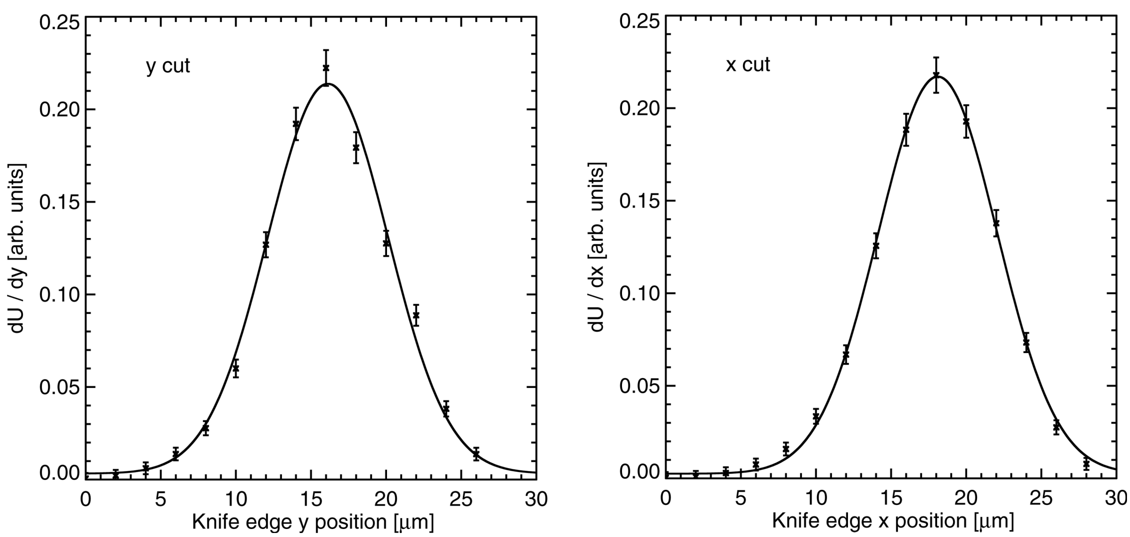

Fig. 4. Derivative of transmitted pulse energy with respect to knife edge position versus knife edge position when the knife edge is translated through the focal waist in two orthogonal directions. The solid curves are best-fit Gaussian profiles corresponding to waist sizes of $7.9 \pm 0.1\,\mu\text{m}$ in the y direction and $8.0 \pm 0.1\,\mu\text{m}$ in the x direction.

The waist is the same size in air or silica, but the Rayleigh range is n times longer in silica than in air. The beam waist deduced from the best fit value for z_R was $8.2 \pm 0.2\,\mu$m, in good agreement with the knife edge value of $7.95 \pm 0.1\,\mu$m.

The third harmonic light can be considered to have three contributions: one from the air before and after the window, one from the input face of the window, and one from the exit face [37]. This approximation holds as long as the coherence length for the third harmonic in silica is much less than the Rayleigh range of the focus. The phase mismatch in silica is

$$\Delta k = k_{3\omega} - 3k_{\omega} = 0.469/\mu\text{m}, \qquad (4)$$

giving a coherence length of $z_{\text{coh}} = 6.7\,\mu$m, which, as required, is much less than the Rayleigh range of $274\,\mu$m for an $8\,\mu$m waist in silica. If the waist is near the input face and the window is much thicker than the Rayleigh range, the third harmonic contribution from the exit face can be ignored. The contribution from air is likewise negligible, so the third harmonic is, to a good approximation, generated right at the input face. Similarly if the waist is near the exit face, the contributions from air and the entrance face can be ignored.

We measure the 1064 nm pulse energy using a pyroelectric detector that is calibrated against a volume absorber thermopile. The accuracy of the pulse energy measurements is $\pm 4\%$. Combined with the beam area uncertainty of 3% and the uncertainty in power deduced from the time profile of 2%, the inferred irradiance at the center of the beam is accurate to $\pm 6\%$.

As we discuss in Section 6, reliable damage threshold measurements require the optical power to be well below both the self-focusing power and the SBS threshold power. This mandates a tight focus, with $w_\circ \le 10\,\mu$m, for 8 ns pulses. For the 14 ps pulses, SBS is not an issue but self-focusing is, and a small waist is still required. For most of our measurements, we used the 1 in focal length lens to focus to a beam waist of approximately $8\,\mu$m, but we sometimes used the 2 in focal length lens to focus to approximately $16\,\mu$m.

Optical damage by the 8 ns pulses is detected by noting a precipitous drop in the transmitted light at the time of breakdown, using a fast photo tube to monitor the transmitted light. This method was not used in the 14 ps measurements because the time resolution of the detector is insufficient. However, breakdown also produces a flash of white light for both 8 ns and 14 ps pulses that we detected using a photomultiplier. In addition, a pilot He–Ne beam probes the 1064 nm focus and severely distorts when damage has occurred.

4. Self-Focusing Corrections

Most transparent materials have a small positive intensity-dependent contribution to the refractive index. For a Gaussian beam this causes a phase advance in the high irradiance center of the beam relative to the low irradiance edges, leading to power-dependent focusing. If the power is greater than the critical self-focusing power, P_{SF}, this focusing overcomes diffraction, and the beam eventually collapses to a tiny diameter, typically leading to filamentary optical damage. When the power is less than P_{SF}, diffraction is not overcome, and the beam does not collapse. However, a focused beam is still affected by incipient self-focusing that alters the position and size of the focal waist. The waist of a Gaussian beam is both reduced in size and moved downstream by amounts that depend on the light power and the distance of the nominal focus behind the input face.

The power required to optically damage silica is high enough that the effects of self-focusing cannot be ignored. Assuming optical damage always occurs first at the spatial location with highest irradiance, it is necessary to understand how self-focusing affects the position and irradiance at that point.

Self-focusing has been thoroughly studied in the literature [29,38,39], but extracting the adjustments to the waist position and the peak irradiance from those studies is not always straightforward. For that reason we developed our own numerical propagation model for a focused Gaussian beam in a medium with an instantaneous Kerr nonlinearity. It uses a split-step fast Fourier transform method with a 256×256 or 512×512 transverse grid and several hundred z steps per Rayleigh range to achieve a high accuracy in the focal region. As expected, for a lowest-order Gaussian beam focused inside a silica window, the Kerr effect leads to a downstream shift in the point of highest irradiance and an increase in the peak irradiance. Figure 6 shows an example from our simulations. This example is for a beam whose low-power focus lies two Rayleigh ranges behind

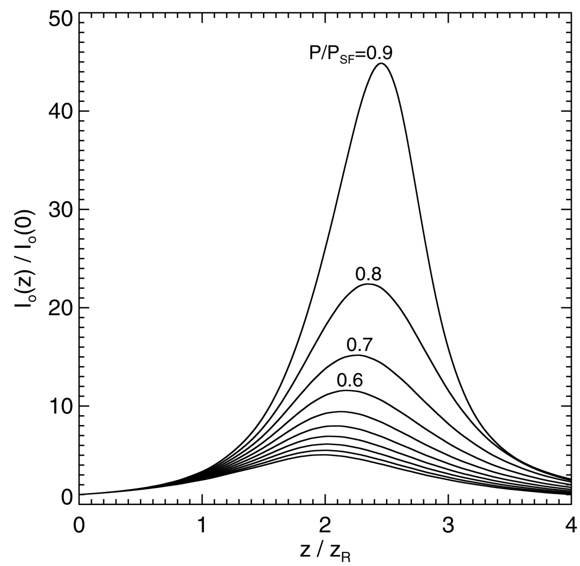

Fig. 6. On-axis irradiance versus position for a beam that is focused two Rayleigh ranges inside a window. With increasing power the position of maximum irradiance moves downstream and the enhancement of the irradiance increases.

the input face of the window. The curves show the on-axis irradiance as a function of distance inside the sample, normalized to the on-axis irradiance at the input face. At low power the focus lies at $z/z_R = 2$, where the normalized irradiance peaks at a value of 5 as expected for a Gaussian focus [40]. As the power is increased, the maximum irradiance point moves farther into the sample, and the peak irradiance is enhanced. For example, at $P/P_{\mathrm{SF}} = 0.7$, the peak irradiance lies at $z/z_R = 2.27$ where the normalized irradiance is 15, a self-focusing enhancement of 3.

Figure 7 shows a plot derived from our model of the maximum normalized irradiance versus P/P_{SF} for different depths of the nominal focus. When the focus coincides with the input face of the window ($z_\circ = 0$), there is little enhancement due to self-focusing. As the focus is moved deeper into the sample, the enhancement grows until, for $z_\circ > 3z_R$, the enhancement closely follows the law

$$\frac{I}{I_\circ} = \frac{1}{1 - P/P_{\mathrm{SF}}}, \tag{5}$$

where I is the peak irradiance with self-focusing included, and $I_\circ$ is the peak irradiance in the absence of self-focusing. The self-focusing power P_{SF} found using our model is

$$P_{\mathrm{SF}} = \frac{0.149\lambda^2}{n_2 n}, \tag{6}$$

where n is the linear refractive index, n_2 is the nonlinear refractive index in units of m^2/W, and λ is the wavelength in vacuum. This expression agrees within 1% with that deduced by Dawes and Marburger [30] from similar numerical studies.

Figure 8 shows the location of the highest irradiance point (z_{Max}) versus power for different nominal focal depths. The curves for $z_\circ > 0$ agree with the self-similar theory of self-focusing [38], which predicts the position of the self-focus point at $P = P_{\mathrm{SF}}$ will move downstream by z_R/m for a beam focused m Rayleigh ranges into the window ($z_\circ = mz_R$). The curve for $z_\circ = 0$ indicates that the point of highest irradiance for a beam focused exactly on the surface lies on the surface if the power is less than $0.25P_{\mathrm{SF}}$ but moves deeper into the window for higher powers. Input face damage measurements should be reliable for $P < 0.25P_{\mathrm{SF}}$ because the peak irradiance lies at the surface. For higher powers caution is needed in interpreting damage measurements as true surface damage.

For exit face damage measurements, the focal shift is insignificant if the window is thicker than $10z_R$. However, the wave reflected from an uncoated exit face has an irradiance equal to 3.4% of the input irradiance when $n = 1.45$. The backward and forward going waves interfere constructively near the exit face, enhancing the field by a factor of 1.18 compared with the forward wave alone. This corresponds to an irradiance enhancement of 40% near the exit face that must be accounted for in interpreting exit face surface damage measurements. In addition, the reflected wave slightly increases the self-focusing of the forward wave, further enhancing the irradiance.

In reality, self-focusing in silica is not quite as simple as described above, because there are two contributions to n_2: one from the electronic Kerr effect, which is instantaneous on the nanosecond scale and well accounted for by our model, and the other due to electrostriction, which is not instantaneous.

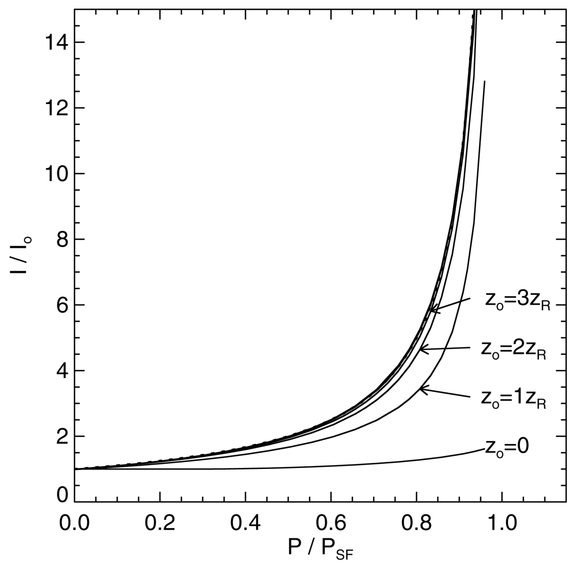

Fig. 7. Irradiance enhancement factor due to self-focusing. The dashed curve corresponds to $1/(1 - P/P_{\mathrm{SF}})$. The other curves correspond to varying enhancement factors derived from numerical modeling for focusing depths of zero, one, two, three, four, and five times the Rayleigh range z_R.

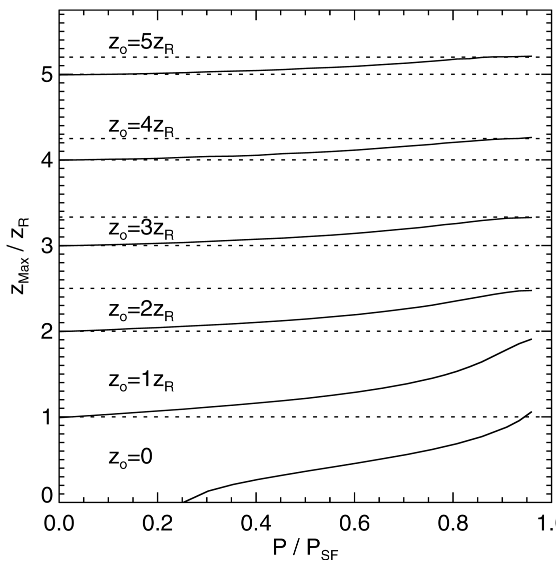

Fig. 8. Position of the maximum irradiance point for varying power with different nominal focusing depths $z_\circ$. The shift in position from $P/P_{\mathrm{SF}} \ll 1$ to $P/P_{\mathrm{SF}} \approx 1$ is approximately $1/z_\circ$, except when $z_\circ = 0$.

The electrostrictive contribution to the CW value of n_2 can be calculated from the mechanical stiffness and $dn/d\rho$ for silica, where ρ is the density of silica. It is independent of the light polarization and has the value $n_2^{es} = 0.57 \times 10^{-20}\,\mathrm{m}^2/\mathrm{W}$ [41]. The speed of longitudinal sound waves in silica is $6 \times 10^3\,\mathrm{m/s}$, so for our $8\,\mu\mathrm{m}$ focal spot, the shortest electrostrictive response time is 1.3 ns. This means electrostriction may fully respond to our 8 ns pulses, but it will be negligible for our 14 ps pulses. The Kerr contribution has been measured many times using various techniques, and the consensus value [42–49] is $n_2^{\mathrm{Kerr}} = 2.1 \pm 0.3 \times 10^{-20}\,\mathrm{m}^2/\mathrm{W}$ for linearly polarized light. For circularly polarized light n_2^{Kerr} is reduced [50] by a factor of 1.5. The values of P_{SF}, including both the electrostrictive and Kerr contributions, for linearly and circularly polarized light are summarized in Table 1.

5. Stimulated Brillouin scattering

It is likely that SBS plays a role in many surface and bulk damage threshold measurements. A simplified model for calculating the SBS threshold of a focused Gaussian beam sets the SBS gain coefficient to 21:

$$g_B I_{\mathrm{SBS}} L_{\mathrm{eff}} = 21, \tag{7}$$

where I_{SBS} is the SBS threshold irradiance, g_B is silica's Brillouin gain coefficient of $5 \times 10^{-11}\,\mathrm{m/W}$, and L_{eff} is an effective gain length. For a beam focused inside the window such that the surfaces are several Rayleigh ranges from the waist, L_{eff} can be set equal to the Rayleigh range. Using

$$L_{\mathrm{eff}} = z_R = w_\circ^2 k/2, \tag{8}$$

and relating the beam power to the on-axis irradiance at the focus

$$I_{\mathrm{SBS}} = 2P_{\mathrm{SBS}}/\pi w_\circ^2, \tag{9}$$

gives an approximate SBS threshold power that is independent of the waist size,

$$P_{\mathrm{SBS}} = 21\lambda/2g_B. \tag{10}$$

For 1064 nm light

$$P_{\mathrm{SBS}} \approx 0.22\,\mathrm{MW}. \tag{11}$$

This approximate model assumes the light is CW. The decay time for the acoustic SBS wave in silica is approximately 5 ns, so for our 8 ns pulses the threshold power should be increased to roughly 0.5 MW. The important point is not the precise threshold value, but that SBS has a power threshold that is independent of the strength of focus, as long as the Rayleigh range is much less than the sample thickness. In fact, we measure a threshold of 0.85 MW for the peak power of our 8 ns pulses, and as predicted we find it is nearly independent of the waist size as long as the focus lies several Rayleigh lengths from either window surface.

This last condition is violated for weakly focused beams, in which case the effective SBS gain length is the window thickness rather than the Rayleigh range. The CW threshold irradiance at the center of a collimated beam is

$$I_{\mathrm{SBS}} = \frac{21}{g_B L}, \tag{12}$$

and to keep I_{SBS} smaller than the damage threshold reported in Section 6 requires $L < 100\,\mu\mathrm{m}$ for a CW beam or $L < 200\,\mu\mathrm{m}$ for an 8 ns pulse.

The SBS threshold is increased for shorter pulses such as our 14 ps pulse, or by phase modulating a long pulse using a modulation period that is short compared with the transit time through the focus in the case of a tight focus or the transit time through the window in the case of a weak focus.

We note that in our study, the SBS threshold is more than a factor of 2 lower for unseeded pulses than for seeded pulses. The spectral broadening of the unseeded laser pulses is insufficient to strongly suppress SBS, yet the light reflected from the back surface contains spectral components that can seed a Stokes wave.

The implication of the SBS threshold estimate is that a reliable damage threshold measurement requires the power to be less than 0.85 MW for a tightly focused 8 ns beam. Of course the irradiance must exceed the damage threshold, and for our 8 ns pulse we find that the waist must be less than $12\,\mu\mathrm{m}$ to cause damage without triggering SBS. For a weakly focused beam, the sample must be thinner than a few hundred micrometers to cause damage without triggering SBS. Many, perhaps most, measurements of silica damage thresholds appear to violate these conditions, so one must keep in mind the possibility that SBS affects them.

6. Measured Bulk Damage Thresholds

We measured bulk damage thresholds for two waist sizes and two pulse durations. We began by describing the results for the 8 ns pulse focused to

Table 1. Self-Focusing Power

Conditions	Nonlinear Coefficient	Self-Focusing Power
Linear, no electrostriction	$n_2 = 2.23 \times 10^{-20}\,\mathrm{m}^2/\mathrm{W}$	$P_{\mathrm{SF}} = 5.20\,\mathrm{MW}$
Circular, no electrostriction	$n_2 = 1.49 \times 10^{-20}\,\mathrm{m}^2/\mathrm{W}$	$P_{\mathrm{SF}} = 7.80\,\mathrm{MW}$
Linear, with electrostriction	$n_2 = 2.73 \times 10^{-20}\,\mathrm{m}^2/\mathrm{W}$	$P_{\mathrm{SF}} = 4.25\,\mathrm{MW}$
Circular, with electrostriction	$n_2 = 1.99 \times 10^{-20}\,\mathrm{m}^2/\mathrm{W}$	$P_{\mathrm{SF}} = 5.84\,\mathrm{MW}$

$w_\circ = 7.5\,\mu$m. We followed with results for the 14 ps pulse focused to 8 μm and for the 8 ns pulse focused to $w_\circ = 16.0\,\mu$m.

We used two procedures to determine a damage threshold. In one the focus dwells on a single location in the sample, and starting with a low pulse energy, we slowly increased it until damage occurred. In the second we set the pulse energy slightly above the damage threshold and noted the power at the instant the transmitted beam was cut off by optical breakdown. Comparing these two should reveal any cumulative damage or annealing effect. The focus is typically 10 Rayleigh ranges deep in the sample to avoid the possibility of surface damage and also to minimize the focal shift due to self-focusing. The second procedure is faster, so it is the one we usually use.

A. Threshold Irradiance or Fluence?

Figure 9 shows the transmitted 1064 nm light for various pulse energies near the damage threshold. The lowest energy pulse is slightly below the optical breakdown threshold, so the full pulse is transmitted. The higher energy pulses damage the silica, causing abrupt termination of transmission at the moment of optical breakdown. It is clear from the traces that there is little or no induction time associated with the breakdown, so damage occurs at a nearly fixed power level rather than at a fixed fluence level. We interpret this to mean that for 8 ns pulses, there is a nearly fixed optical breakdown irradiance, assuming there is no direct dependence on the size of the focus. We test this assumption in Subsection 6.G and Section 7. For picosecond pulses this is probably not true and fluence may be more appropriate. Throughout this paper we quote the damage threshold as a full pulse fluence even though breakdown occurs before the end of the pulse and even though irradiance is more appropriate for the longer pulses.

B. Statistical or Deterministic Threshold?

With the power set a few percent above the damage threshold, we find the power at the point of breakdown is always the same within the 1% uncertainty of our relative power measurement. There is no statistical variation in the damage threshold. Furthermore there is no variation among the several grades of fused silica we tested.

However, if we block the injection seeder so the Nd:YAG laser operates on multiple longitudinal modes, the damage threshold fluence falls by a factor of 4, and the damage becomes statistical. This is due solely to the statistical nature of the multilongitudinal-mode pulses in accord with the claims of Glebov *et al.* [5,6]. A comparison of damage statistics for single and multilongitudinal mode is shown in Fig. 10. In this case we start with a pulse energy above threshold and slowly decrease it in small steps. At each power level we allow 3000 pulses to reach the sample. The probability of damage after the 3000 pulses is plotted versus fluence expressed as an equivalent irradiance. The equivalent irradiance is the on-axis fluence converted to irradiance using the measured beam size and including a self-focusing correction but ignoring power fluctuations of unseeded pulses. The probability step for seeded pulses is less than 1% full width, but that for the unseeded pulses is approximately 10%. The factor of 4 reduction in threshold fluence and the factor of 10 increase in the step size agrees well with simulations of the peak irradiance associated with the fine time structure of unseeded pulses. This structure fluctuates from pulse to pulse, reflecting the fluctuations in the quantum starting noise for the different longitudinal modes

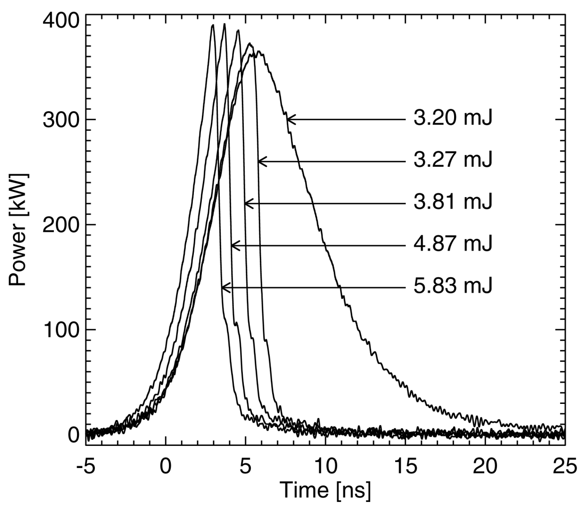

Fig. 9. Transmitted power near the damage threshold of fused silica for an 8.1 μm focal waist. The 3.20 mJ trace corresponds to subthreshold power. The higher energy traces show that damage is sudden and occurs at a nearly constant power. There is a small increase in power at breakdown with increasing pulse energy, indicating a nonzero damage induction time. The detector/scope bandwidth is 4 GHz.

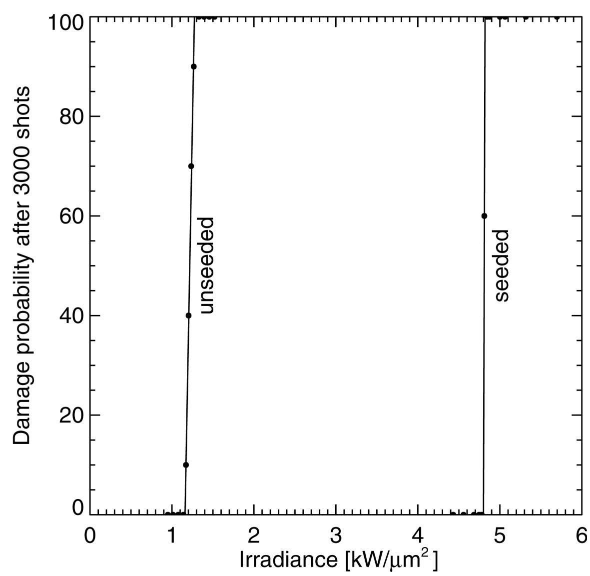

Fig. 10. Probability of bulk optical damage in silica after 3000 pulses at a single focal location versus peak irradiance. The transition near 4.8 kW/μm^2 is for seeded single longitudinal mode pulses. The lower transition is for unseeded multimode pulses.

of the laser. For a 30 GHz linewidth and a mode spacing of 250 MHz, the highest spikes in the multimode pulses are four to six times as intense as the maximum of a seeded pulse of the same energy, in agreement with the measured factor of 4 reduction in threshold. The width of the step is associated with the statistical nature of the power spikes in unseeded pulses.

This interpretation assumes that the damage occurs on a time scale comparable to, or shorter than, the spikes of the multimode pulses. The width of a typical spike is roughly 15 ps, corresponding to the 30 GHz laser linewidth. This implies that damage occurs on a time scale of 15 ps or less. We will see that this is indeed true when we discuss damage by the 14 ps pulses. The interpretation also assumes that the longitudinal modes of the laser operate independently, so the time structure can be described by a model of independent modes that start from quantum noise. We tested this by comparing the surface third harmonic signal from seeded and unseeded pulses. A pulse comprised of a large number of independent modes would generate six times as much third harmonic as a single-mode pulse of the same energy. We measured a ratio of 5.5 and concluded that the modes do operate almost independently of one another.

As a direct test for the existence of damage precursors, we focused the seeded laser pulse to a 7.5 μm waist lying 2.9 mm deep in a 10 mm thick silica window and set the pulse energy to 90% of the damage threshold. While the laser operated at 10 pulses per second, we scanned the sample in the transverse direction at a rate of 100 μm/s for a total distance of 180 mm, exposing an area of approximately 2 mm^2. We observed no white light emission on any shot that might indicate damage. We subsequently examined the sample under a microscope using strong side lighting that highlights damaged spots and found no indication of material modification or bulk damage at any point in the sample. This verifies our less formal observation that in tens of thousands of damage tests, we never observed breakdown at less than the intrinsic threshold. Clearly the bulk damage that we measure is always an intrinsic damage and is never caused by damage precursors or defects in the silica. This is true of all the grades of silica that we tested.

C. Cumulative Damage or Conditioning?

We have not found either a significant cumulative damage or annealing effect. Further we find there is little variation in the damage threshold from one spot to another in a single sample or from one sample to another, including different grades of fused silica. We appear to be measuring a true intrinsic damage threshold that is highly deterministic, varying by at most 1% from point to point. Just at the limit of our measurement precision, there may be a slight annealing effect. The damage threshold may increase by 1% to 3% with repeated irradiation of a single point by subthreshold pulses.

As a check for cumulative bulk damage, we fixed a 7.5 μm focus at one location in a sample and ran the laser at 10 pulses per second with the pulse energy set to 90% of the damage threshold for 15,000 shots. The sample was not damaged.

D. Electron Avalanche

The maximum amplitude of the optical field at the measured bulk breakdown threshold of 4.8 kW/μm^2 is 1.57 GV/m. This is close to the measured DC intrinsic breakdown threshold of 1.3 GV/m measured by Yasue [17] using probe microscopy on a 13 nm thick silica layer grown on a silicon wafer. Of course the DC measurement has an external source of charged carriers, whereas the laser-induced breakdown must generate its own electrons. Apart from any difference caused by that, the expected ratio for 1064 nm versus DC fields is

$$E_{1064\,\mathrm{nm}} = E_{DC}\sqrt{2(1+\omega^2\tau_c^2)}, \tag{13}$$

where ω is the optical frequency, and τ_c is the time between momentum changing collisions of an electron. The square root term accounts for the reduced electron heating rate of an oscillating field compared with a DC field. Assuming a collision time of 0.25 fs, the threshold optical field predicted from the DC field is 2.0 GV/m, comparable to the measured damage threshold field of 1.57 GV/m. We interpret this comparison as strongly supportive of the electron avalanche explanation of optical damage.

E. Self-Focusing Correction

The self-focusing correction is expected to be approximately 10% for the 8 μm focus. We can test our understanding of self-focusing by varying the distance of the focus behind the entrance face of the sample. Figure 11 shows the measured damage threshold powers versus focus location for the 8 μm focal waist. The measured values are indicated by the symbols, and the solid curve shows the computed curve for the self-focusing correction. The correction in this case is about 10%, but for larger focal sizes the threshold power and self-focusing correction would be larger. Figure 12 shows a similar comparison for the 16.5 μm focal waist. The details of the fit are not as nice as for the 8 μm waist, but the values at the surface and deep in the window have the expected ratio. The cause of the imperfect agreement at intermediate focal positions is uncertain. It might be caused by the slower electrostrictive response for the larger beam, or it may be that SBS affects the measurement. SBS is slightly above threshold for the deepest focus but just at or slightly below threshold for the surface focus. Small deviations of the transverse beam profile from a Gaussian may also contribute to the imperfect agreement.

We have assumed in these tests that the surface damage threshold, measured at $z = 0$, is equal to the bulk damage threshold. We verify this in Section 7.

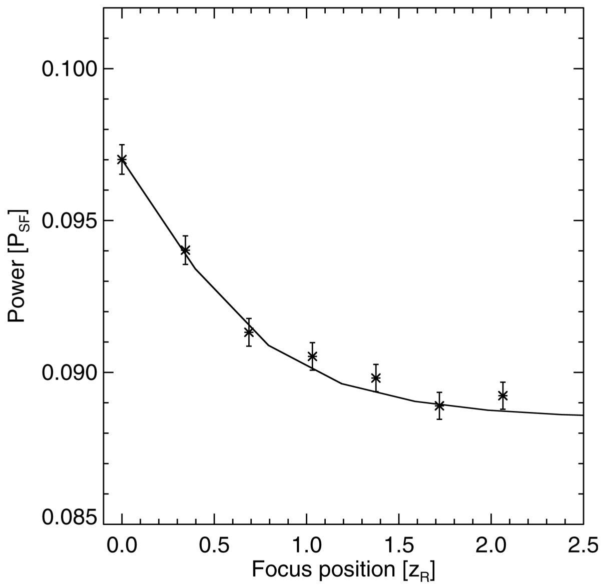

Fig. 11. Measured and computed damage threshold powers illustrating weak self-focusing. The symbols are measured damage threshold powers in units of P_{SF} versus the position of focus relative to the entrance surface in units of the Rayleigh range, and the solid curve is computed using our numerical model of self-focusing. The measured Rayleigh range is $z_R = 254\,\mu\text{m}$ in silica, and we assume $P_{SF} = 4.26\,\text{MW}$.

F. SBS Threshold

We measured the SBS threshold for focal waists of 15 and 49 μm and found little change in the threshold power. It was 850 kW in both cases. For these tight focusing conditions, the Stokes wave is a phase conjugate of the pump wave, and we find that it propagates back through the pin hole filters and into the laser where it is amplified and refocused onto the sample with a 30 ns time delay. We analyzed the prompt and delayed pulses using a Fabry–Perot etalon and verified a Stokes shift of approximately −15 GHz for the delayed pulse. The Stokes wave is usually generated late in the pump pulse as expected for the 5 ns memory time of the acoustic wave. For the 15 and 49 μm beams, the presence of SBS did not strongly affect the measured damage threshold. However, we do not cite the resulting values, because the presence of SBS casts doubt on their accuracy. We use only the 8 μm results, where damage occurs well below the SBS threshold. Although SBS did not appear to affect the damage thresholds for the 15 and 49 μm beams, this is not an indication that it would not strongly influence thresholds for larger diameter beams where the Stokes wave could focus within the sample and cause damage.

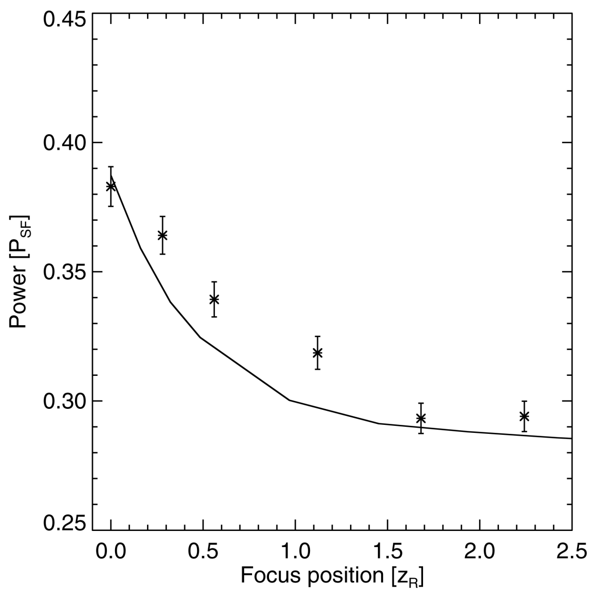

Fig. 12. Measured and computed damage threshold powers illustrating moderate self-focusing. The symbols are measured damage threshold powers in units of the self-focusing power and the Rayleigh range, and the curve is computed using our numerical model of self-focusing. The measured Rayleigh range is $z_R = 1035\,\mu\text{m}$ in silica, and we assume $P_{SF} = 4.26\,\text{MW}$.

G. Size Effect

We looked for an effect of focal spot size on the damage threshold in two ways. As described above we compared the damage threshold irradiance for the 8 ns pulses using different focal waist sizes and found no noticeable difference for the 8 μm and 16 μm waists, but because the damage threshold power for the 16 μm waist is slightly above the SBS threshold, we cannot be sure there is no difference between them. However, we can state that the threshold irradiance is not lower for the larger focal spot, contrary to the usual claim.

We also sought evidence of a size effect by placing a curved mirror after the sample to reflect the transmitted beam back through the focus. This forms a standing wave at the focus whose antinodes are nearly four times as intense as the forward wave alone. The reimaging is not perfect, owing to optical imperfections and because it does not accommodate the small amount of self-focusing. Nevertheless this is a useful check on the existence of a size effect on the scale of one-fifth of a micrometer, the distance between a peak and a valley in the standing wave. We find that the incoming pulse energy required to cause damage is approximately one-third that needed for single-pass damage. This is approximately 25% more than expected if there was no size effect and the reimaging was perfect. Part of the difference is due to the imperfect reimaging, but part may be caused by diffusion of the electron energy from the peaks toward the valleys of the standing wave, which would reduce the electron avalanche rate. A more quantitative measure of this effect is discussed in Section 7.

H. Polarization Effect

We compared the damage thresholds for linear and circularly polarized light using 8 ns pulses focused to 8 μm. After taking account of the differing self-focusing corrections, we found no measurable difference in the damage thresholds.

I. Pulse Duration Effect

We compared damage thresholds for the 8 ns and 14 ps pulses focused to 8 μm, looking for a duration effect to compare with a $\tau^{0.5}$ or similar scaling law for the threshold damage fluence. As described in Section 3, the time profile of the 8 ns pulse is measured using a fast photo tube and oscilloscope. The 14 ps pulse is characterized by an autocorrelation measurement. The full width at half maximum, assuming a $\mathrm{sech}^2(t/\tau)$ pulse shape, is 14 ps, while assuming an e^{-2t^2/τ^2} pulse shape, it is 15 ps. We again used surface third harmonic generation to measure the focal spot size and to position the focus, and we used white light emission as the damage indicator.

Our measured threshold damage fluence is 2.3×10^{-7} J/μm^2 for the 14 ps pulse compared with 4.1×10^{-5} J/μm^2 for the 8 ns pulse. This value takes into account the time dependence of the self-focusing enhancement of the focal irradiance. Our 8 ns and 14 ps measurements are added to the previously presented results as the filled circles in Fig. 13. The ratio of threshold fluences for our two measurements is 180 compared with the ratio of pulse durations of 570. If a $\tau^{0.5}$ dependence were correct, it would imply a fluence ratio of 24 rather than 180. The maximum irradiance for the 14 ps pulses at threshold is 3.1 times higher than for the 8 ns pulses. As Fig. 13 shows, our 8 ns threshold lies quite near that predicted from the DC breakdown voltage [17] and well above most previously reported values.

J. Strain Effect

In polarization-maintaining fibers a strain-induced birefringence is used to maintain the polarization. The birefringence is roughly $\Delta n = 10^{-4}$. We squeezed cubes of silica in a press to induce strain and birefringence similar to that in fibers. Birefringence and strain are related by

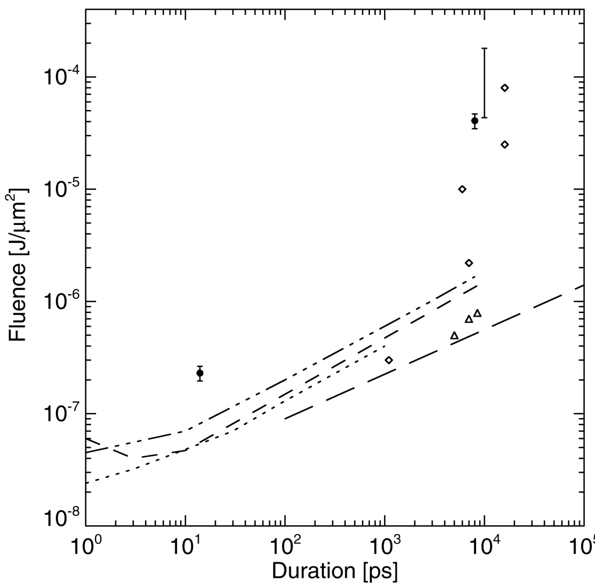

Fig. 13. Same data as Fig. 1 with our two measured values added as filled circles.

$$\Delta\left(\frac{1}{n^2}\right)_{ij} = \rho_{ijkl}e_{kl}, \tag{14}$$

where ρ_{ijkl} is the elasto-optic tensor, e_{kl} is the strain defined by

$$e_{kl} = \frac{1}{2}\left(\frac{\partial u_k}{\partial x_l} + \frac{\partial u_l}{\partial x_k}\right), \tag{15}$$

and u_i is the displacement in the i direction. The strain e_{kl} in turn is related to applied stress σ_{kl} by

$$e_{ij} = s_{ijkl}\sigma_{kl}, \tag{16}$$

where s_{ijkl} is the compliance tensor. If a compressive force is applied to the x face in the x direction, the only nonzero stress is σ_{xx}, which produces strains e_{xx}, e_{yy}, and e_{zz} and changes in n_x and n_y, given by

$$\Delta n_x = -\frac{n_x^3}{2}(\rho_{xx}e_{xx} + \rho_{xy}e_{yy} + \rho_{xz}e_{zz}), \tag{17}$$

$$\Delta n_y = -\frac{n_y^3}{2}(\rho_{yy}e_{yy} + \rho_{yx}e_{xx} + \rho_{yz}e_{zz}), \tag{18}$$

where the elasto-optic tensor coefficients for silica have dimensionless values $\rho_{xx} = \rho_{yy} = \rho_{zz} = 0.121$ and $\rho_{xy} = \rho_{yz} = \rho_{xz} = 0.270$. The birefringence can be written as

$$\Delta n_x - \Delta n_y = \frac{n^3}{2E}\sigma_{xx}(\rho_{xy} - \rho_{xx})(1 + \nu), \tag{19}$$

where $E = 73$ GPa is Young's modulus, and $\nu = 0.164$ is Poisson's ratio for silica. Thus

$$\Delta n_x - \Delta n_y = \frac{1.45^3}{2 \times 7.3 \times 10^{10}}(0.149)(1.164)\sigma_{xx}, \tag{20}$$

$$\Delta n_x - \Delta n_y = 3.6 \times 10^{-12}\sigma_{xx}. \tag{21}$$

σ_{xx} is negative for compression in the x direction. A birefringence of $\Delta n_y - \Delta n_x = 10^{-4}$ requires $\sigma_{xx} = 2.8 \times 10^7$ Pa (1 Pa = 1 N/m^2) or a compressive force of 28 N/mm^2.

Rather than trying to set the birefringence to 10^{-4}, it was more convenient to adjust the pressure to a half-wave retardation between x and y polarized 633 nm light from a He–Ne laser. For our 12.8 mm × 12.8 mm × 12.8 mm silica cubes, this requires $\Delta n = 2.5 \times 10^{-5}$, which implies $\sigma_{xx} = 6.9 \times 10^6$ Pa corresponding to a pressure of 6.9 N/mm^2. We adjusted the pressure of our press to achieve the half-wave retardation over a stripe at the center of the silica cube and focused the laser beam to an 8 μm waist positioned 2.9 mm behind the front face. We measured the damage threshold for 1064 nm light polarized parallel and perpendicular to the strain. These are the eigen polarization directions for the strained cube, so there is no depolarization inside the silica. We found no measurable difference in the damage thresholds of unstrained and strained silica for either polarization.

K. White Light Emission

Figure 14 shows a typical time profile of the white light emitted by silica on bulk breakdown by an 8 ns pulse focused to 8 μm, with the pulse energy set slightly above the damage threshold. The short initial spike appears immediately after the transmission of the 1064 nm light is terminated by breakdown. It is not scattered or reflected laser light, because we block the 1064 nm light at the detector. It is probably black body light emitted by the hot plasma associated with damage. The plasma can cool by releasing pressure through fracturing and by propagation of a pressure wave away from the damage zone. The cooling time would be approximately equal to the size of the fracture divided by the acoustic velocity, or 15 ns, which is comparable to the observed duration of the short pulse. There might be light emitted from the pressure front and from the fracturing material as well. The longer lower level white light peak is probably black body radiation emitted as the lattice further cools by conduction. The white light has been examined in more detail by others [51] who confirm a black body emission for the short pulse with a temperature of 10,000 K and for the long tail with a temperature of 5000 K. The thermal diffusion time for a hot cylinder in silica is $\tau = 1.1 \times 10^{-6} r^2$, or perhaps 100 μs in our case. This cooling time is consistent with the slow decay of the white light. The maximum energy deposited in the plasma was 1.5 mJ, assuming all the laser light arriving after plasma ignition was absorbed by the plasma.

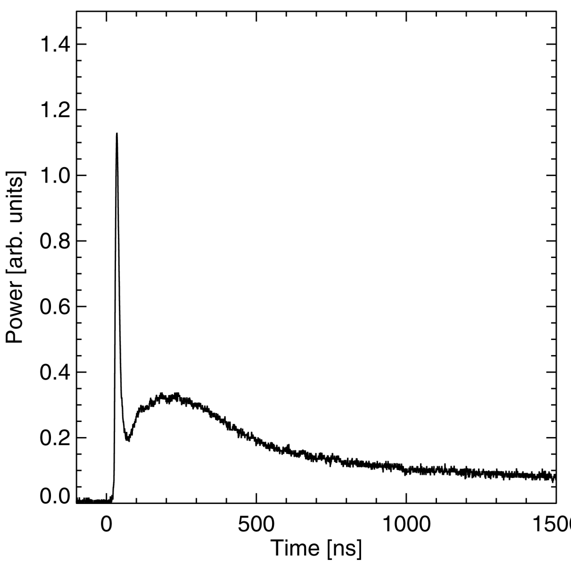

Fig. 14. Time profile of white light emitted after optical breakdown of silica by an 8 ns pulse.

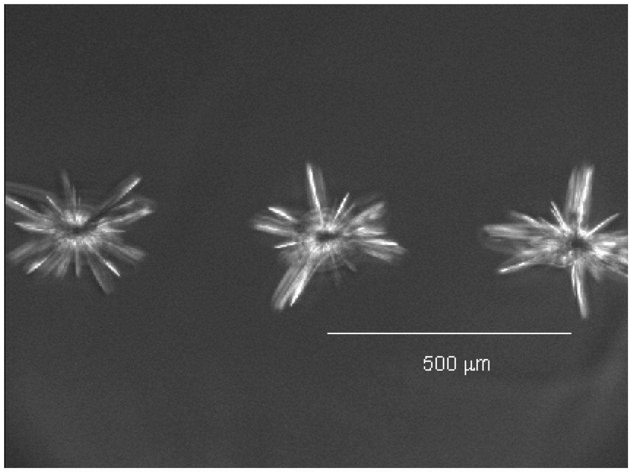

Fig. 15. End view of bulk optical damage of fused silica at three locations by 8 ns single longitudinal mode pulses. The images are produced by a phase contrast microscope. The pattern indicates multiple radial fracture planes.

L. Damage Morphology

Figures 15 and 16 show end and side view images of the damage caused by three consecutive 8 ns pulses focused to 8 μm with the pulse energy set just above the damage threshold. These images were made using a phase contrast microscope. The end view shows a set of fractures radiating from the focus. In the side view of Fig. 16, these fractures form the bloomlike upper part of the damage. The light propagation direction is upward in the side view, and the focal waist is located at the center of the fracture zone. There is a tubelike structure extending upstream approximately 150 μm from the waist, and the tube terminates with

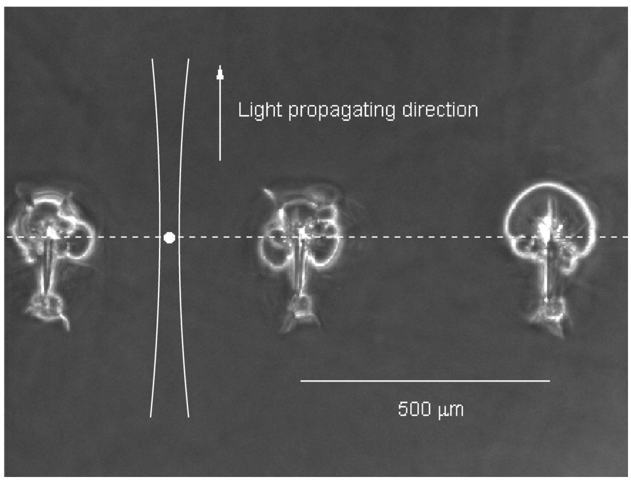

Fig. 16. Side view of bulk optical damage of fused silica at three locations for 8 μm focal waist and 8 ns single longitudinal mode pulses with energy slightly above the breakdown threshold. The curves qualitatively indicate the shape of the beam as it passes through the focus, and the size of the dot indicates the uncertainty in the location of the focus. Breakdown occurs first at the focus where a large bloom of radial fractures is centered and propagates upstream. An apparent tube begins at the focus and extends approximately one Rayleigh range upstream to the point where damage stalls and a smaller bloom is formed.

another smaller fracture zone. The tube is probably a melted and resolidified region with a slightly elevated refractive index.

We hypothesize that breakdown occurs initially at the exact location of the focus. After breakdown the resulting plasma can absorb the incoming light at its upstream boundary. The boundary moves upstream until the irradiance is insufficient to sustain a plasma, which is approximately one Rayleigh range. After the plasma stalls, additional energy from the trailing edge of the pulse causes the fractures at the termination point.

The minimum energy required to excite the critical density of 10^9 electrons per cubic micrometer by 10 eV over the damage volume of $2 \times 10^4\,\mu\mathrm{m}^3$ is

$$U_{\mathrm{plasma}} = (10^9 e/\mu m^3)(2 \times 10^4\,\mu m^3)(10\,\mathrm{eV}/e) \times (1.6 \times 10^{-19}\,\mathrm{J/eV}) = 30\,\mu J \mu J. \quad (22)$$

This critical electron density makes the plasma frequency equal to the light frequency for 1064 nm light, but it involves only 1% of the available electrons. The energy required to raise an amount of silica equal to the volume of the tube to the softening point of 1600 C is only 25 μJ. The 1.5 mJ available for absorption is thus ample for ionizing and melting the tube and also creating considerable additional damage such as fracturing.

Figure 17 shows a side view of damage under similar conditions except a larger 17 μm focus is used and the pulse energy is approximately 25% above the damage threshold. The only fracturing in this case is at the upstream end of the damage trail. This implies that the damage moves upstream quickly after the initial damage at the focus, so most of the energy in the pulse is absorbed at the upstream end of the trail. This damage morphology is also reproducible from pulse to pulse. Damage by the 14 ps pulses is also reproducible as a single filament that extends upstream from the focal waist by roughly one Rayleigh range. The high degree of reproducibility of damage morphology for each measurement condition strongly refutes initiation by randomly dispersed impurity inclusions.

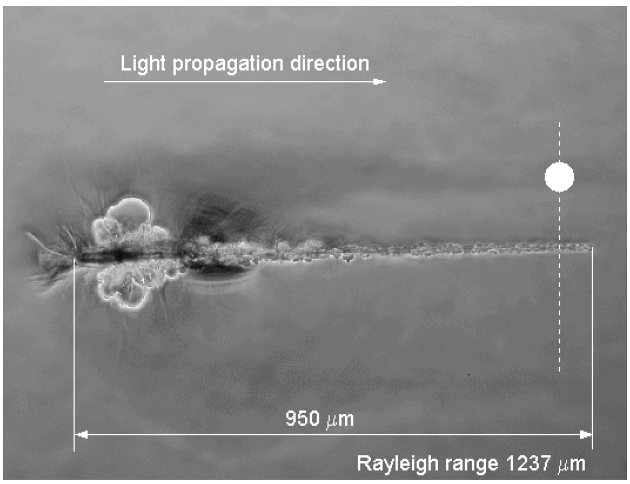

Fig. 17. Side view of bulk optical damage of fused silica for a 17 μm focal waist and an 8 ns single longitudinal mode pulse with energy 25% above the breakdown threshold. Breakdown is initiated at the focus and propagates upstream approximately one Rayleigh range.

7. Surface Damage Measurements

The quality of the surface polish is known to strongly influence surface damage thresholds, so we tried a variety of polishing methods in search of any that might raise the surface damage threshold to the bulk level.

Figure 18 shows single shot damage threshold irradiances for 8 ns pulses with the beam focused on the front surface to an 8 μm waist. We set the pulse energy slightly above the bulk damage level, and the irradiance at breakdown is deduced from the power at the time of transmission cutoff. Three polishes were tested: a standard ceria polish, an alumina polish with a final grit size of 100 nm, and the same alumina polish followed by a 40 nm grit silica polish. The alumina polish is rated 5–10 for scratch and dig, which is less fine than a super polish. We find that the surface breakdown threshold for the ceria-polished windows is always less than the bulk damage threshold and averaged approximately 1.5 $\mathrm{kW}/\mu\mathrm{m}^2$, or about one-third of the bulk value. The lowest threshold of the 20 measured spots was 0.50 $\mathrm{kW}/\mu\mathrm{m}^2$, or one-tenth, the bulk value. The alumina-polished part damaged at the bulk level for approximately 50% of the spots tested, but at the remaining spots the damage threshold averaged approximately 50% of the bulk value. The fact that 50% of the spots damage at the bulk level is promising, because it suggests that a better finish might have reduced the concentration of surface fractures and scratches to yield a more uniformly high threshold. We did achieve a nearly uniform threshold equal to the bulk threshold by following the alumina polish with a silica polish. Only one of 20 spots tested on this sample had a damage threshold lower than the bulk value.

There is a qualitative difference in damage morphology between the spots that damage at the bulk level and those that damage below the bulk level. In the former the damage consists of multiple radial fractures, similar in end view to the interior bulk

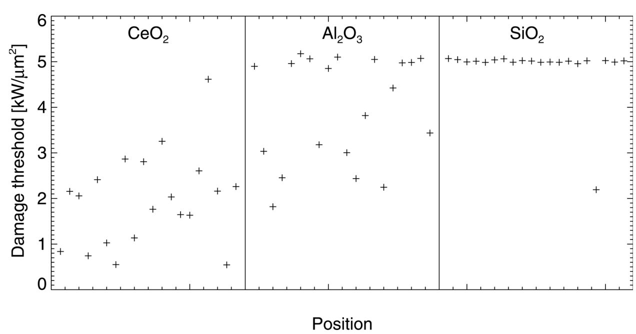

Fig. 18. Single shot damage threshold irradiance for 8 ns pulses on silica polished using ceria, alumina, and alumina followed by silica.

damage. In the latter there is no fracturing, and the damage appears as a dimple in the surface. Presumably, in low threshold cases, a plasma is ignited near the surface, either from material ejected from the surface or at surface scratches and cracks, and this plasma quickly spreads into the air in front of the window, preventing the irradiance at the surface from reaching the bulk damage level.

Figure 19 shows damage thresholds for the ceria- and alumina-polished windows measured by slowly increasing the pulse energy from a low value until damage occurred. Compared with the single-pulse results presented above, we see that the damage threshold for the ceria-polished sample fell to a fairly uniform value of $1.0\,\mathrm{kW}/\mu\mathrm{m}^2$, lower than many of the single shot values. In contrast, slowly ramping up the pulse energy appears to improve the performance of the alumina-polished sample. Only one of 12 spots tested this way had a threshold significantly below the bulk level.

We also measured exit surface damage thresholds for silica-polished samples. Exit face thresholds are expected to be lower than bulk damage thresholds, because the wave reflected from the exit face creates a standing wave near the exit face with peak irradiances that are approximately 40% stronger than for the forward-traveling wave alone. This leads to the expectation that the exit face damage threshold pulse energy should be 71% of the bulk threshold. In fact, we find it is slightly higher than this, at $81 \pm 1\%$ of the bulk threshold. This difference might be attributed to diffusion of the electron energy away from the peaks toward the valleys of the standing wave. In Section 1 we claimed a hot electron diffusion length of approximately $0.5\sqrt{\tau}\,\mu\mathrm{m}$ where τ is a time measured in nanoseconds. For $\tau = 30\,\mathrm{ps}$, typical of the growth time for the electron density with our 8 ns pulses, this gives a diffusion length of 100 nm, which is comparable to the 183 nm distance from an irradiance peak to the neighboring valleys. Such diffusion might cool the electrons so a slightly higher optical field is required to achieve breakdown. Whether or not this is the correct explanation, the higher than expected exit face damage threshold is good news for high-power applications.

We also looked for a variation of surface damage thresholds with size of the beam at the silica-polished surface. We focused to $7.5\,\mu$m and varied the position of the focus from exactly on the input face to two Rayleigh ranges in front of the surface. This varies the area of the beam at the surface by a factor of 5. We found that damage occurs at exactly the same on-axis surface irradiance for all beam sizes as shown in Fig. 20. The measured thresholds, indicated by symbols, are matched well by the solid curve computed, assuming a focal waist of $7.7\,\mu$m, in close agreement with the $7.5\,\mu$m waist deduced from a surface third harmonic measurement. There is no SBS in this measurement, and self-focusing is irrelevant.

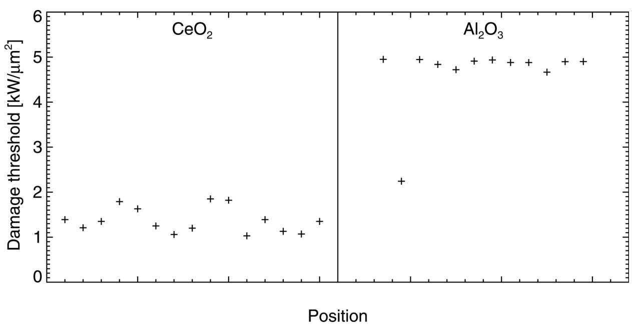

Fig. 19. Annealed damage irradiance for 8 ns pulses on silica polished using ceria and alumina.

8. Breakdown of Air

The distance between the focus in air and the front face of the window in Fig. 20 was limited by air breakdown. For distances greater than $1.7z_R$, the air broke down before the surface was damaged, protecting the surface. We measured the probability of air breakdown for these focusing conditions and obtained the data shown in Fig. 21. The air breakdown fluence at the focus is approximately 3.3 times that of silica for seeded pulses. For unseeded pulses the air breakdown threshold is approximately two times smaller than for the seeded pulses. This reduction is smaller than the factor of 4 between seeded and unseeded thresholds for silica, so for unseeded pulses the air breakdown fluence is approximately seven times higher than the unseeded silica breakdown threshold. These air breakdown fluences are comparable to the literature values, but they are more precise, because our beam size is known well [52]. The smaller ratio of seeded to unseeded thresholds for air compared with silica is due to a longer electron re-

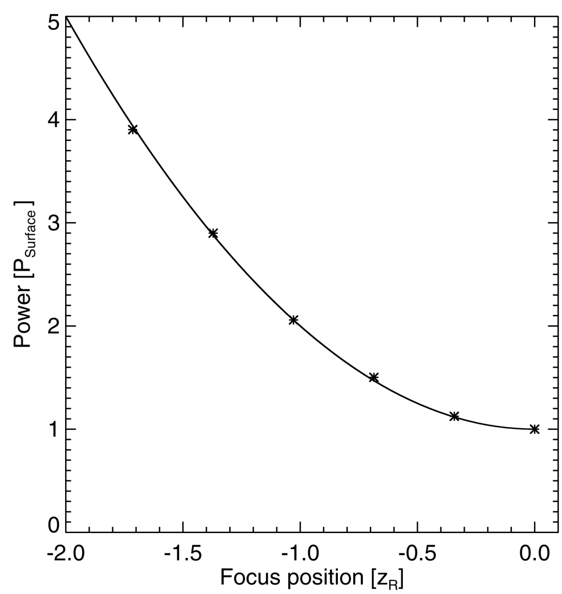

Fig. 20. Symbols are measured damage threshold powers in units of the surface damage threshold power at the beam waist, plotted against the distance of the focus from the input face of the window, measured in units of the Rayleigh range ($w_\circ = 7.68\,\mu$m and $z_R = 174\,\mu$m). The solid curve is computed from the focusing equation in air. No dependence of damage threshold on beam size is seen.

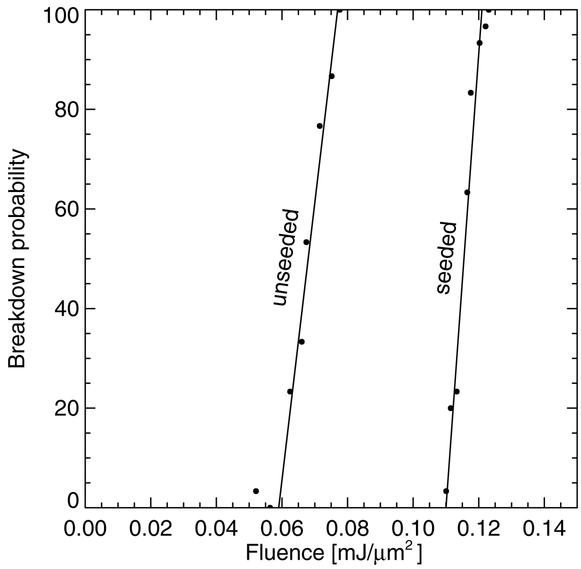

Fig. 21. Probability of air breakdown versus fluence at a $w_\circ = 7.5\,\mu$m focus for seeded and unseeded 8 ns pulses. Each point represents the probability of breakdown based on 30 pulses.

combination time in air than in silica. Near threshold the air breakdown occurs well into the trailing half of the laser pulse where the power is as low as 30% of its peak value. At higher pulse energies the moment of breakdown occurs earlier in the pulse. This delayed air breakdown near threshold allowed us to extend the silica damage measurements shown in Fig. 20 somewhat beyond the air breakdown fluence. The signatures of breakdown for air are similar to those for silica. The transmission of the 1064 nm light abruptly and totally terminates, and a flash of white light is emitted. Our air breakdown measurements were taken with several seconds between laser pulses in open air at an elevation of 1650 m above sea level.

9. Rate Equation Model of Electron Avalanche

The nature of breakdown shown in Fig. 9 for 8 ns pulses, where breakdown always occurs at the peak of the pulse when barely above the damage threshold and slightly before the peak of the pulse when well above threshold, indicates that electron growth is extremely rapid once the irradiance exceeds the damage threshold, but there is little or no avalanche growth when the irradiance is below the threshold. This can be explained by a large electron loss rate in the following rate equation describing the avalanche growth of free electrons:

$$\frac{\mathrm{d}n}{\mathrm{d}t} = \beta I^k + \alpha n I - \frac{n}{\tau_r}. \tag{23}$$

Here τ_r is the electron–hole recombination lifetime, α is the electron avalanche growth coefficient, and βI^k is the multiphoton ionization source term. This source term may be responsible for providing the seed electrons, but it is otherwise relatively unimportant in the avalanche growth for 8 ns pulses. If τ_r is much shorter than the pulse duration ($\tau_r \ll 10^{-8}$ s), then any avalanche growth, which requires $\alpha I > 1/\tau_r$, implies $\alpha I \gg 10^8\,\mathrm{s}^{-1}$. At the threshold of avalanche growth where the growth and loss terms balance, the growth term must already be large to counter the large recombination rate. A slight increase in I above the balance point would thus lead to rapid avalanche growth with a growth time much less than the pulse duration. At the damage threshold $\alpha\tau_r = 1/I_{\mathrm{th}} = 2.1 \times 10^{-4}\,\mu\mathrm{m}^2/\mathrm{W}$.

The fast recombination term has not usually been included in electron avalanche rate equations for nanosecond pulses. However, rapid recombination has been measured in several femtosecond studies of silica, with deduced recombination times in the range of 50–300 fs. The presence of the large loss rate explains the observation of Shen *et al.* [20] that there is no growth of the free electron density when the irradiance is less than the damage threshold. This observation has been the basis of arguments that optical damage in silica is not caused by an electron avalanche.

We numerically integrated the rate equation, varying the three coefficients β, α, and τ_r to best fit our measurements, for the 8 ns and 14 ps pulses. We first tried to match the transmitted pulse shapes as the energy of the 8 ns pulses is varied above the damage threshold. At an electron density of $n = 2 \times 10^8/\mu\mathrm{m}^3$, the absorption length becomes submicrometer, so we use this as the damage criterion in this exercise. We varied τ_r, keeping the product $\alpha\tau_r$ fixed at $2.1 \times 10^{-4}\,\mu\mathrm{m}^2/\mathrm{W}$, and found that $\tau_r = 250$ fs gave the breakdown powers and times indicated by the diamond symbols in Fig. 22. We concluded that τ_r must lie in the vicinity of 250 fs with an uncertainty of 75 fs. This value for τ_r implies $\alpha = 8.4 \times 10^8\,\mu\mathrm{m}^2/\mathrm{J}$. The coefficients used for the results plotted in Fig. 22 were $\alpha = 8.34 \times 10^8\,\mu\mathrm{m}^2/\mathrm{J}$, $\tau_r = 250$ fs, and $\beta = 2 \times 10^{-19}\,\mu\mathrm{m}^{13}/\mathrm{W}^8\mathrm{s}$.

We next used these rate coefficients to model breakdown fluence versus pulse duration, obtaining the solid curve shown in Fig. 23. It fits the 14 ps data

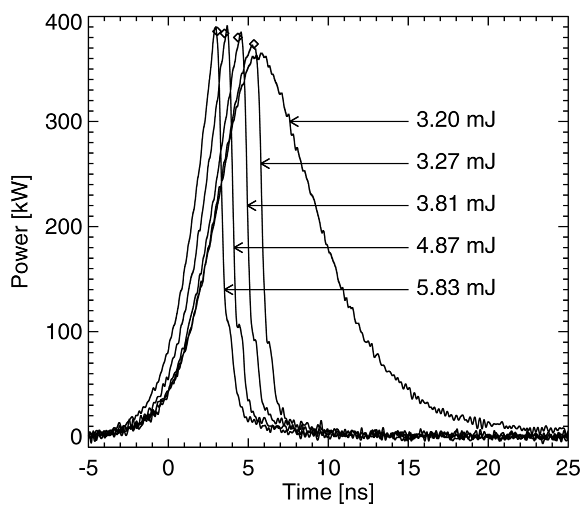

Fig. 22. Same data as Fig. 9 with rate equation predictions indicated by diamonds.

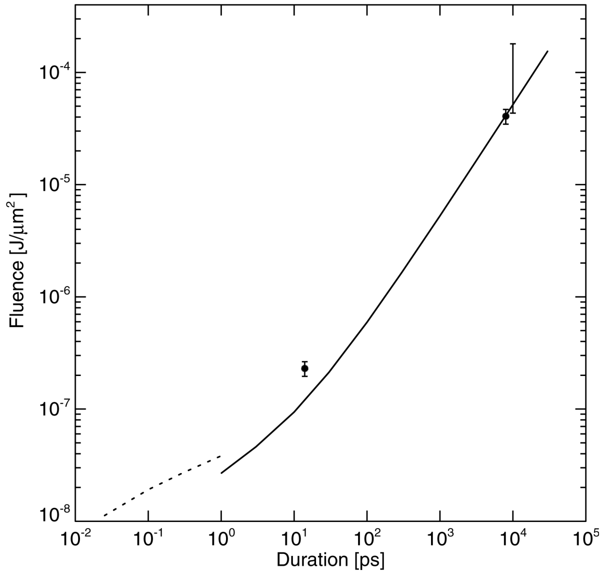

Fig. 23. Our measured (symbols) and modeled values (solid curve), Mero *et al.* [57] values for 800 nm light (dashed curve), and the value deduced from the DC breakdown voltage (vertical bar).

point reasonably well, underestimating the threshold at 14 ps by only a factor of 2. A better fit to our two data points could be achieved by adjusting the rate coefficients slightly, but that may be placing more credence in the simple rate equation model than it merits. The slope of the computed curve is unity for pulses longer than 50 ps, indicating a linear dependence of threshold fluence on pulse duration. For pulses shorter than 50 ps, the slope is lower, becoming approximately 0.5 at 1 ps.

In the rate equation model, we used the lowest value of β that is consistent with the photoionization of a large number of free electrons within the focal volume in the time before the avalanche begins to grow. This requirement is suggested by our observation that there is no statistical variation in the breakdown such as might be expected if there were a small number of seed electrons. Thus $\beta I_{\mathrm{th}}^8 \tau V \gg 1$, where V is the volume within which damage is initiated, I_{th} is the threshold irradiance for 8 ns pulses, and τ is the time of transition from electron loss to growth during which the seed electrons must be created. The minimum value of β is best found by numerical integration of the rate equation, but we can estimate it using $V = 50\,\mu\mathrm{m}^3$, which implies $\beta > 7 \times 10^{-32}/\tau\,\mu\mathrm{m}^{13}/\mathrm{W}^8$. If we use $\tau = 1$ ps we have $\beta > 7 \times 10^{-20}\,\mu\mathrm{m}^{13}/\mathrm{W}^8\mathrm{s}$. In the numerical integration we find the slightly larger value $\beta = 2 \times 10^{-19}$ produces the necessary density of free electrons to start the avalanche, but β cannot be much smaller than this, or the statistical variation in the number of seed electrons would be noticeable.

It is interesting to compare our rate coefficients with those deduced by other researchers. Several previous studies have applied similar electron avalanche rate models to optical damage over the femtosecond to second range. Audebert *et al.* [53] measured the phase shift caused by free electrons in a femtosecond pump/probe measurement, and concluded $\tau_r = 150$ fs. This was supported by Sun *et al.* [54] who used shadow microscopy and found $\tau_r = 150$ fs, by Mao *et al.* [55] who used phase shift measurements to find $\tau_r \approx 100$ fs, and by Li *et al.* [56] who used double pulse damage threshold studies to deduce $\tau_r \approx 60$ fs. Mero *et al.* [57] measured damage thresholds of thin film silica for 20–1000 fs pulses and fit their measurements with a rate equation model that set $\tau_r = 220$ fs. Quere *et al.* [58] also give convincing evidence of the ≈100 fs recombination time in silica. Clearly there is ample support for our deduced electron lifetime of roughly 250 fs. It is interesting to note that the loss of free electrons, according to these studies, is not simply a cooling of hot electrons but a recombination causing electron loss. The recombination process is not necessarily well understood. Petite *et al.* [59] agree with an electron recombination lifetime of 150 fs, but they attribute it to formation of self-trapped excitons with energies lying in the bandgap. These excitons, or maybe just a fraction of them, are claimed to decay with a lifetime of a nanosecond or so. No matter what the recombination process might be, we can state that the trapped or recombined electrons must be nearly as difficult to ionize as the valence band electrons.

We know of only one other rate equation for silica damage for light with a wavelength near 1064 nm that can be used to compare the photoionization coefficients β. That is from the study of Stuart *et al.* [23] that used 1053 nm pulses. Most other studies used 800 nm light, which ionizes with six photons rather than eight and should have much larger ionization rates. Stuart *et al.* give a coefficient of $\beta = 9 \times 10^{-22}\,\mu\mathrm{m}^{13}/\mathrm{W}^8\mathrm{s}$. This is 220 times smaller than ours. However, considering that they did not include an electron loss rate that would require a higher ionization rate to counter it, and considering that the ionization rates would be equal for coefficients with a ratio of 220 with only a factor of 2 difference in irradiances, this disagreement seems relatively insignificant.

That leaves only a comparison of α's, the avalanche rate. This rate should be nearly the same for 800 and 1964 nm light, according to Eq. (13). All the studies in [3,23,56–58] give coefficients in the range of $3–9 \times 10^8\,\mu\mathrm{m}^2/\mathrm{J}$, in good agreement with our value of $8.34 \times 10^8\,\mu\mathrm{m}^2/\mathrm{J}$.

The study by Mero *et al.* [57] presented especially high-quality measurements of damage in films of silica on bulk silica using 800 nm pulses with durations of 25 fs to 1 ps. Their derived rate coefficients were $\tau_r = 220$ fs and $\alpha = 8 \times 10^8$, both of which agree well with our values. We have included their damage thresholds in Fig. 23 as the dashed curve. With slight adjustments, perhaps due to the difference in wavelengths, our curve splices onto theirs quite well, indicating that an avalanche model with fixed rate coefficients can describe the intrinsic damage threshold of silica from a few femtoseconds to many nanoseconds.

Finally we note that our measurements indicate that linear and circular polarizations have equal damage thresholds when their different self-focusing corrections are included. This is not blindingly obvious since multiphoton absorption can have a polarization dependence, and perhaps avalanche heating can as well. Furthermore Bhardwaj *et al.* [60] report striking changes in silica surface damage morphology caused by changing the polarization angle of linearly polarized femtosecond light pulses.

10. Damage by Larger Diameter Beams

Many measurements of optical damage to silica use beams with diameters of $300\,\mu$m or more. The damage threshold fluence is typically a factor of 50 lower than those we report here. We did not have sufficient pulse energy to produce damage with such large beams, so we have no direct observations in this regime. However, we can point out that such large beams will produce strong SBS unless the light is strongly phase modulated to raise the SBS threshold or unless the sample is thinner than $300\,\mu$m. The power required to produce damage with such large beams will also be several times larger than P_{SF}, so self-focusing may be important. Large beams also have Rayleigh ranges much larger than the sample thickness, making the measurement sensitive to surface damage. Even for our best polish with silica, large beams might have a high probability of including a surface spot that has a low threshold. It is not known whether the silica surface polish can be perfected to reduce this probability to near zero. A better understanding of intrinsic damage with large beams requires that measurements use temporally smooth beams with stable and high-quality spatial profiles, monitoring for SBS and self-focusing, and that high-threshold surface polishes be further developed.

11. Conclusions

Based on the observations reported in this paper, we make the following claims regarding damage of silica by 1064 nm light:

1. Bulk damage of silica is deterministic and intrinsic when a tight focus is used. The threshold irradiance for 8 ns pulses is $4.75 \pm 0.25\,\mathrm{kW}/\mu\mathrm{m}^2$. There is no evidence of damage initiation by damage precursors or of a thermal nature of damage initiation. The variation in damage threshold from point to point in a sample and from sample to sample is less than the 1% pulse-to-pulse variation of our seeded laser.
2. There is no accumulation of damage from exposure to subthreshold pulses. There may be a slight conditioning effect, but if so it is near the detection limits of our measurements.
3. The input surface damage threshold can be made equal to the bulk damage threshold. This was achieved most reliably by using an alumina or silica polish. Less reliable was annealing an alumina-polished surface, although higher quality alumina polishes may perform better than those used here. Ceria polishes are clearly inferior in damage threshold, and they suffer from cumulative damage. The silica polish appears to leave a silica layer that may not provide the optical quality or ruggedness required for some applications. Nevertheless it proves that surfaces can be as resistant to optical damage as the bulk.
4. The only measurable size effect was found when a retroreflected beam created a standing wave inside the sample. The small but clear increase in the threshold irradiance in this situation may be a consequence of electron diffusion over the 180 nm distance between neighboring irradiance peaks and valleys. Over the range of our 8–16 μm foci, we could detect no size effect apart from this.
5. Breakdown behavior is consistent with a three term electron avalanche model. Pulses longer than 100 ps have a nearly constant breakdown field that is consistent with the measured DC breakdown field. The three rates in the avalanche model that best fit our measurements are remarkably similar to those deduced for femtosecond to picosecond pulses and include a 250 fs recombination term. The three-term avalanche model thus works well from a few femtoseconds to many nanoseconds and beyond. The $\sqrt{\tau}$ dependence of the intrinsic damage threshold fluence in the picosecond to nanosecond range is refuted.
6. Tight focusing is required for spectrally narrow nanosecond pulses if SBS is to be kept below threshold. SBS may be responsible, in part, for the much lower damage thresholds usually reported in the literature. Because SBS is statistical it may also account for the statistical nature of damage that is claimed for nanosecond pulses but not for femtosecond pulses. SBS can be suppressed by broadening the spectrum as an alternative to using a tight focus.
7. The role of self-focusing has been verified as agreeing with our numerical model. Our results are consistent with other theoretical treatments.
8. Mechanical strain at the level encountered in polarization-maintaining optical fiber has no effect on the damage threshold.
9. The polarization state of the light has no effect on the intrinsic damage threshold.
10. For an 8 ns pulse focused to 8 μm, the breakdown threshold of air is several times that of silica, so air breakdown does not limit the optical power that can be transmitted into a fiber or a window for this size beam.
11. The morphology of bulk damage indicates that breakdown always ignites exactly at the focus and propagates upstream. Damage morphology is reproducible from pulse to pulse.

We thank Alpine Research Optics and D. Collier and R. Schuster for supplying windows with different surface polishes. We also thank A. Kilgo of Sandia National Laboratories for advice and assistance on silica polishing. This work was supported by the United States Department of Energy (DOE) under contract DE-AC04-94AL85000. Sandia is a multiprogram laboratory operated by Sandia Corporation, a Lockheed

Martin Company, for the United States Department of Energy.

References

1. D. Arnold and E. Cartier, "Theory of laser-induced free-electron heating and impact ionization in wide-band-gap solids," Phys. Rev. B **46**, 15102–15115 (1992).
2. N. Bloembergen, "Laser-induced electric breakdown in solids," IEEE J. Quantum Electron. **10**, 375–386 (1974).
3. M. Lenzner, J. Kruger, S. Sartania, Z. Cheng, C. Spielmann, G. Mourou, W. Kautek, and F. Krausz, "Femtosecond optical breakdown in dielectrics," Phys. Rev. Lett. **80**, 4076–4079 (1998).
4. M. J. Soileau, W. E. Williams, N. Mansour, and E. W. Van Stryland, "Laser-induced damage and the role of self-focusing," Opt. Eng. **28**, 1133–1144 (1989).
5. L. B. Glebov, O. M. Efimov, G. T. Petrovskii, and P. N. Rogovtsev, "Influence of the mode composition of laser radiation on the optical breakdown of silicate glasses," Sov. J. Quantum Electron. **14**, 226–229 (1984).
6. L. B. Glebov, "Intrinsic laser-induced breakdown of silicate glasses," Proc. SPIE **4679**, 321–330 (2002).
7. L. Lamaignere, S. Bouillet, R. Courchinoux, T. Donval, M. Josse, J.-C. Poncetta, and H. Bercegol, "An accurate, repeatable, and well characterized measurement of laser damage density of optical materials," Rev. Sci. Instrum. **78**, 103105 (2007).
8. S. Webster, F. C. McDonald, A. Villanger, M. J. Soileau, E. W. Van Stryland, D. J. Hagan, B. McIntosh, W. Toruellas, J. Farroni, and K. Tankala, "Optical damage measurements for high peak power ytterbium doped fiber amplifiers," Proc. SPIE **5991**, 599115 (2005).
9. D. W. Fradin and M. Bass, "Comparison of laser-induced surface and bulk damage," Appl. Phys. Lett. **22**, 157–159 (1973).
10. J. Neauport, L. Lamaignere, H. Bercegol, F. Pilon, and J.-C. Birolleau, "Polishing-induced contamination of fused silica optics and laser induced damage density at 351 nm," Opt. Express **13**, 10163–10171 (2005).
11. F. Y. Genin, A. Salleo, T. V. Pistor, and L. L. Chase, "Role of light intensification by cracks in optical breakdown on surfaces," J. Opt. Soc. Am. B **18**, 2607–2616 (2001).
12. E. W. Van Stryland, M. J. Soileau, A. L. Smirl, and W. E. Williams, "Pulse-width and focal-volume dependence of laser-induced breakdown," Phys. Rev. B **23**, 2144–2151 (1981).
13. H. Varel, D. Ashkenasi, A. Rosenfeld, R. Herrmann, F. Noack, and E. E. B. Campbell, "Laser-induced damage in SiO_2 and CaF_2 with picosecond and femtosecond laser pulses," Appl. Phys. A **62**, 293–294 (1996).
14. D. Kitriotis and L. D. Merkle, "Multiple pulse laser-induced damage phenomena in silicates," Appl. Opt. **28**, 949–958 (1989).
15. L. D. Merkle, N. Koumvakalis, and M. Bass, "Laser-induced bulk damage in SiO_2 at 1.064, 0.532, and 0.355 μm," J. Appl. Phys. **55**, 772–775 (1984).
16. A. E. Chmel, "Fatigue laser-induced damage in transparent materials," Mater. Sci. Eng. B **49**, 175–190 (1997).
17. T. Yasue, Y. Yoshida, H. Koyama, T. Kato, and T. Nishioka, "Dielectric breakdown of silicon dioxide studied by scanning probe microscopy," J. Vac. Sci. Technol. B **15**, 1884–1888 (1997).
18. J. Bude, G. Guss, M. Mathews, and M. L. Spaeth, "The effect of lattice temperature on surface damage in fused silica optics," Proc. SPIE **6720**, 672009 (2007).
19. A. M. Rubenchik and M. D. Feit, "Initiation, growth and mitigation of UV laser induced damage in fused silica," Proc. SPIE **4679**, 79–95 (2002).
20. X. A. Shen, S. C. Jones, and P. Braunlich, "Laser heating of free electrons in wide-gap optical materials at 1064 nm," Phys. Rev. Lett. **62**, 2711–2713 (1989).
21. T. Q. Jia, H. X. Chen, M. Huang, F. L. Zhao, X. X. Li, S. Z. Xu, H. Y. Sun, D. H. Feng, B. B. Li, X. F. Wang, R. X. Li, Z. Z. Xu, X. K. He, and H. Kuroda, "Ultraviolet-infrared femtosecond laser-induced damage in fused silica and CaF_2 crystals," Phys. Rev. B **73**, 054105 (2006).
22. N. Kuzuu, K. Yoshida, H. Yoshida, T. Kamimura, and N. Kamisugi, "Laser-induced bulk damage in various types of vitreous silica at 1064, 532, 355, and 266 nm: evidence of different damage mechanisms between 266 nm and longer wavelengths," Appl. Opt. **38**, 2510–2515 (1999).
23. B. C. Stuart, M. D. Feit, S. Herman, A. M. Rubenchick, B. W. Shore, and M. D. Perry, "Nanosecond-to-femtosecond laser-induced breakdown in dielectrics," Phys. Rev. B **53**, 1749–1761 (1996).
24. R. R. Austin, R. Michaud, A. H. Guenther, and J. Putman, "Effects of structure, composition, and stress on the laser damage threshold of homogeneous and inhomogeneous single films and multilayers," Appl. Opt. **12**, 665–676 (1973).
25. T. R. Moore, G. L. Fischer, and R. W. Boyd, "Measurement of the power distribution during stimulated Brillouin scattering with focused Gaussian beams," J. Mod. Opt. **45**, 735–745 (1998).
26. H. Yoshida, H. Fujita, and M. Nakatsuka, "Stimulated Brillouin scattering phase-conjugated wave reflection from fused-silica glass without laser-induced damage," Opt. Eng. **36**, 2557–2562 (1997).
27. J. M. Sajer, "Stimulated Brillouin scattering and front surface damage," Proc. SPIE **5273**, 129–135 (2004).
28. J. R. Murray, J. R. Smith, R. B. Ehrlich, D. T. Kyrazis, C. E. Thompson, T. L. Weiland, and R. B. Wilcox, "Experimental observation and suppression of transverse stimulated Brillouin scattering in large optical components," J. Opt. Soc. Am. B **6**, 2402–2411 (1989).
29. J. H. Marburger, "Self-focusing: theory," Prog. Quantum Electron. **4**, 35–110 (1975).
30. E. L. Dawes and J. H. Marburger, "Computer studies in self-focusing," Phys. Rev. **179**, 862–868 (1969).
31. A. C. Tien, S. Backus, H. Kapteyn, M. Murnane, and G. Mourou, "Short-pulse laser damage in transparent materials as a function of pulse duration," Phys. Rev. Lett. **82**, 3883–3886 (1999).
32. D. Du, X. Liu, G. Korn, J. Squier, and G. Mourou, "Laser-induced breakdown by impact ionization in SiO_2 with pulse widths from 7 ns to 150 fs," Appl. Phys. Lett. **64**, 3071–3073 (1994).
33. B. C. Stuart, M. D. Feit, A. M. Rubenchik, B. W. Shore, and M. D. Perry, "Laser-induced damage in dielectrics with nanosecond to subpicosecond pulses," Phys. Rev. Lett. **74**, 2248–2251 (1995).
34. J. H. Campbell, F. Rainer, M. Kozlowski, C. R. Wolfe, I. Thomas, and F. Milanovich, "Damage resistant optics for a mega-joule solid-state laser," Proc. SPIE **1441**, 444–456 (1991).
35. R. M. Wood, *Laser-Induced Damage of Optical Materials* (Institute of Physics, 2003).
36. J. F. Ward and G. H. C. New, "Optical third harmonic generation in gases by a focused laser beam," Phys. Rev. **185**, 57–72 (1969).
37. R. J. Gehr and A. V. Smith, "Separated-beam nonphase-matched second harmonic method of characterizing nonlinear optical crystals," J. Opt. Soc. Am. B **15**, 2298–2307 (1998).
38. V. I. Talanov, "Focusing of light in cubic media," JETP Lett. **11**, 199–201 (1970).
39. R. L. Sutherland, *Handbook of Nonlinear Optics* (Marcel Dekker, 1996).
40. A. E. Siegman, *Lasers* (University Science Books, 1986).
41. E. L. Buckland, "Mode-profile dependence of the electrostrictive response in fibers," Opt. Lett. **24**, 872–874 (1999).

42. R. Adair, L. L. Chase, and S. A. Payne, "Nonlinear refractive index of optical crystals," Phys. Rev. B **39**, 3337–3350 (1989).
43. G. Rodriguez and A. J. Taylor, "Measurement of cross-phase modulation in optical materials through the direct measurement of the optical phase change," Opt. Lett. **23**, 858–860 (1998).
44. T. Olivier, F. Billard, and H. Akhouayri, "Nanosecond Z-scan measurements of the nonlinear refractive index of fused silica," Opt. Express **12**, 1377–1382 (2004).
45. F. A. Oguama, H. Garcia, and A. M. Johnson, "Simultaneous measurement of the Raman gain coefficient and the nonlinear refractive index of optical fibers: theory and experiment," J. Opt. Soc. Am. B **22**, 426–436 (2005).
46. D. Milam, "Review and assessment of measured values of the nonlinear refractive-index coefficient of fused silica," Appl. Opt. **37**, 546–550 (1998).
47. A. Melloni, V. Frasca, A. Garavaglia, A. Tonini, and M. Martinelli, "Direct measurement of electrostriction in optical fibers," Opt. Lett. **23**, 691–693 (1998).
48. A. C. Liu, M. J. F. Diggonet, and G. S. Kino, "Measurement of the dc Kerr and electrostrictive phase modulation in silica," J. Opt. Soc. Am. B **18**, 187–194 (2001).
49. K. S. Kim, R. H. Stolen, W. A. Reed, and K. W. Quoi, "Measurement of the nonlinear index of silica-core and dispersion-shifted fibers," Opt. Lett. **19**, 257–259 (1994).
50. R. W. Boyd, *Nonlinear Optics* (Academic, 1992).
51. C. W. Carr, H. B. Radousky, A. M. Rubenchik, M. D. Feit, and S. G. Demos, "Localized dynamics during laser-induced damage in optical materials," Phys. Rev. Lett. **92**, 087401 (2004).
52. Y.-L. Chen, J. W. L. Lewis, and C. Parriger, "Spatial and temporal profiles of pulsed laser-induced air plasma emissions," J. Quant. Spectrosc. Radiat. Transfer **67**, 91–103 (2000).
53. P. Audebert, P. Daguzan, A. Dos Santos, J. C. Gauthier, J. P. Geindre, S. Guizard, G. Hamoniaux, K. Krastev, P. Martin, G. Petite, and A. Antonetti, "Space–time observation of an electron gas in SiO_2," Phys. Rev. Lett. **73**, 1990–1993 (1994).
54. Q. Sun, S. B. Jiang, Y. Liu, Y. H. Zhou, H. Yang, and Q. H. Gong, "Relaxation of dense electron plasma induced by femtosecond laser in dielectric materials," Chin. Phys. Lett. **23**, 189–192 (2006).
55. S. S. Mao, F. Quere, S. Guizard, X. Mao, R. E. Russo, G. Petite, and P. Martin, "Dynamics of femtosecond laser interactions with dielectrics," Appl. Phys. A **79**, 1695–1709 (2004).
56. M. Li, S. Menon, J. P. Nibarger, and S. N. Gibson, "Ultrafast electron dynamics in femtosecond optical breakdown of dielectrics," Phys. Rev. Lett. **82**, 2394–2397 (1999).
57. M. Mero, J. Liu, W. Rudolph, D. Ristau, and K. Starke, "Scaling laws of femtosecond laser induced breakdown in oxide films," Phys. Rev. B **71**, 115109 (2005).
58. F. Quere, S. Guizard, and P. Martin, "Time-resolved study of laser-induced breakdown in dielectrics," Europhys. Lett. **56**, 138–144 (2001).
59. G. Petite, P. Daguzan, S. Guizard, and P. Martin, "Ultrafast processes in laser irradiated wide bandgap insulators," Appl. Surf. Sci. **109–110**, 36–42 (1997).
60. V. R. Bhardwaj, E. Simova, P. P. Rajeev, C. Hnatovsky, R. S. Taylor, D. M. Rayner, and P. B. Corkum, "Optically produced arrays of planar nanostructures inside fused silica," Phys. Rev. Lett. **96**, 057404 (2006).
61. H. Krol, L. Gallais, M. Commandre, C. Grezes-Besset, D. Torricini, and G. Lagier, "Influence of polishing and cleaning on the laser-induced damage threshold of substrates and coatings at 1064 nm," Opt. Eng. **46**, 023402 (2007).
62. J.-Y. Natoli, L. Gallais, H. Akhouayri, and C. Amra, "Laser-induced damage of materials in bulk, thin-film, and liquid forms," Appl. Opt. **41**, 3156–3166 (2002).
63. T. Kamimura, S. Akamatsu, H. Horibe, H. Shiba, S. Motokoshi, T. Sakamoto, T. Jitsuno, T. Okamato, and K. Yoshida, "Enhancement of surface-damage resistance by removing subsurface damage in fused silica and its dependence on wavelength," Jpn. J. Appl. Phys. **43**, L1229–L1231 (2004).
64. J.-Y. Natoli, B. Bertussi, and M. Commandre, "Effect of multiple laser irradiations on silica at 1064 and 355 nm," Opt. Lett. **30**, 1315–1317 (2005).
65. L. D. Merkle and D. Kitriotis, "Temperature dependence of laser-induced bulk damage in SiO_2 and borosilicate glass," Phys. Rev. B **38**, 1473–1482 (1988).